LITHOLOGICAL CONTROLS ON HILLSLOPE SEDIMENT SUPPLY: INSIGHTS FROM LANDSLIDE ACTIVITY AND GRAIN SIZE DISTRIBUTIONS.

Duna C. Roda-Boluda[1]*, Mitch D'Arcy[2], Jordan McDonald[1, †], Alexander C. Whittaker[1]

[1]Department of Earth Science & Engineering, Imperial College London Royal School of Mines, Prince Consort Road, SW7 2BP London, United Kingdom.

[2]Institute of Earth and Environmental Science, University of Potsdam, Karl-Liebknecht-Str. 24-25, 14476 Potsdam-Golm, Germany

* corresponding author: roda@gfz-potsdam.de; d.roda-boluda12@imperial.ac.uk

[†]Now at Risk Management Solutions, 30 Monument Street, EC3R 8NB London, United Kingdom

Short title: Lithologic controls on hillslope sediment supply.

Keywords: Lithology, hillslopes, landslides, grain size, sediment supply

Accepted Article

This article has been accepted for publication and undergone full peer review but has not been through the copyediting, typesetting, pagination and proofreading process which may lead to differences between this version and the Version of Record. Please cite this article as doi: 10.1002/esp.4281

This article is protected by copyright. All rights reserved.

ABSTRACT

The volumes, rates and grain size distributions of sediment supplied from hillslopes represent the initial input of sediment delivered from upland areas and propagated through sediment routing systems. Moreover, hillslope sediment supply has a significant impact on landscape response time to tectonic and climatic perturbations. However, there are very few detailed field studies characterising hillslope sediment supply as a function of lithology and delivery process. Here, we present new empirical data from tectonically-active areas in southern Italy that quantifies how lithology and rock- strength control the landslide fluxes and grain size distributions supplied from hillslopes. Landslides are the major source of hillslope sediment supply in this area, and our inventory of ~2800 landslides reveals that landslide sediment flux is dominated by small, shallow landslides. We find that lithology and rock strength modulate the abundance of steep slopes and landslides, and the distribution of landslide sizes. Outcrop-scale rock strength also controls the grain sizes supplied by bedrock weathering, and influences the degree of coarsening of landslide supply with respect to weathering supply. Finally, we show that hillslope sediment supply largely determines the grain sizes of fluvial export, from catchments and that catchments with greater long-term landslide rates deliver coarser material. Therefore, our results demonstrate a dual control of lithology on hillslope sediment supply, by modulating both the sediment fluxes from landslides and the grain sizes supplied by hillslopes to the fluvial system.

Accepted Article

This article is protected by copyright. All rights reserved.

INTRODUCTION

The characteristics of sediment supplied from hillslopes to channels set the initial boundary conditions for sediment fluxes from upland areas (Allen et al., 2015; Sklar et al., 2016). The rates and grain sizes of hillslope sediment supply can have a significant impact on basin stratigraphy (e.g. Armitage et al., 2011; Allen et al., 2015), and play a crucial role in channel incision processes, thus influencing landscape response time and relief evolution (e.g. Sklar & Dietrich, 2001, 2006; Cowie et al., 2008; Egholm et al., 2013). The volumes, rates and grain size distributions of sediment exported from hillslopes vary greatly depending on the delivery process (e.g. Attal et al., 2015; Sklar et al., 2016), lithology (e.g. Selby et al., 1980; Portenga & Bierman, 2011; Allen et al., 2015), and the degree of weathering and jointing of bedrock (e.g. Selby, 1980; Moore et al., 2009; Clarke & Burbank, 2010; Sklar et al., 2016). However, there are few empirical data sets exploring how these variables control hillslope sediment production and delivery, in contrast with the large body of research studying how this primary sedimentary signal is transformed during transport and deposition (e.g. Jerolmack & Paola, 2010; Simpson & Castelltort, 2012; Michael et al., 2014; Allen et al., 2016).

Here, we present new empirical data addressing lithology and rock strength controls on the fluxes and grain size distributions of sediment delivered from hillslopes to channels, using tectonically-active areas of southern Italy as a case study. We first compile a new landslide inventory along active normal faults, and evaluate the influence of lithology on slope distributions, landslide occurrence, frequency-magnitude relationships and field-calibrated landslide area-volume scaling. We then present new field data on rock strength and landslide controls on the grain size distributions supplied from hillslopes to channels. Finally, we evaluate the effects of hillslope supply on the grain sizes of the fluvial sediment export.

Sediment supply from landslides: lithological controls

Landslides are the only erosional mechanism by which hillslopes can keep pace with fluvial incision once their strength-limited equilibrium slopes are surpassed (e.g. Montgomery & Brandon, 2002; Burbank et al., 1996). Consequently, landslides can account for a significant proportion of hillslope erosion and sediment fluxes over 10^0-10^6

This article is protected by copyright. All rights reserved.

Accepted Article

yr timescales (e.g. Hovius et al., 1997; Guzzetti et al., 2009; Larsen & Montgomery, 2012; Simoni et al., 2013). In response to greater tectonic forcing or fluvial incision, landslide erosion rates can increase through changes in the frequency and/or volumes of mobilized sediment (e.g. Larsen et al., 2010; Korup et al., 2012). Overall, lithology can influence sediment fluxes from landslides by controlling: (a) rock strength, which dictates slope distributions and the critical angles for landsliding; (b) rates of landslide occurrence; (c) frequency distributions of landslide sizes; and (d) landslide area-volume scaling relationships.

It has long been recognized that different rock units have different outcrop- and landscape-scale rock strengths, which reflect the combination of intact strength, degree of weathering, and fracturing (Selby, 1980; Schmidt & Montgomery, 1995; Montgomery & Brandon, 2002). However, quantifying meaningful rock strength values remains a major challenge (Korup, 2008; Moore et al., 2009; Clarke & Burbank, 2010; Gallen et al., 2015). The strength of lithological units can influence slope distributions within a region, and dictate the equilibrium angles that can lead to hillslope failure (e.g. Burbank et al., 1996; Korup, 2008; Korup & Schlunegger, 2009; Clarke & Burbank, 2010) and non-linear increases in erosion rates (Binnie et al., 2007; Ouimet et al., 2009). Lithologies with lower rock strength are characterized by lower equilibrium angles, which can lead to a greater frequency of landslide events (Korup, 2008; Korup & Schlunegger, 2009; Hurst et al., 2013; Borgomeo et al., 2014).

The probability distribution of landslide sizes can be described using a power law (e.g. Hovius et al., 1997; Guzzetti et al., 2002; Malamud et al., 2004a, b). For geomorphological landslide inventories, which reflect cumulative landsliding over an unknown period of time, it is more appropriate to calculate the areal frequency density of landslides, because the total number of landslides is not known, (Malamud et al., 2004a). The total number of landslides cannot be extracted from geomorphological inventories, because some have been eroded, and because constraints on imagery resolution mean smaller landslides are often not mapped (e.g. Stark & Hovius, 2001; Guzzetti et al. 2002, Malamud et al., 2004a). The non-cumulative frequency density of landslides of different sizes, $f(A_L)$ also follows a power law, which can be defined for the number of landslides, N_L over an area A_L as (e.g. Guzzetti et al., 2002; Malamud et al., 2004a):

This article is protected by copyright. All rights reserved.

$$f(A_L) = -\frac{dN_L}{dA_L} = C' A_L^{-\beta} \quad \text{(Equation 1)}$$

In this case, *C'* is a constant that depends on local conditions and landslide rates, and β is the power-law exponent that defines the decay in frequency of bigger landslides. A rollover is typically observed in the frequency-area distributions, which for geomorphological inventories is generally attributed to the incompleteness of the inventory towards smaller landslides (e.g. Stark & Hovius, 2001; Malamud et al., 2004a; Guzzetti et al., 2002; Hurst et al., 2013). Therefore, the fitted power-law is only representative over the range of landslide areas that fall between the rollover value and the area of the largest mapped landslide. From a compilation of 27 landslide inventories, Van Den Eeckhaut et al. (2007) observed that β typically is 2.3 ± 0.6, with smaller values indicating a greater volumetric contribution of large, infrequent landslides to the inventory. Based on empirical and model data, it has been suggested that β is controlled by the depth-gradient of fracture density and cohesion: rock units with greater strength/depth gradients (i.e. considerably less cohesive and more fractured near the surface than at depth), tend to generate shallower, smaller landslides and have greater power-law exponents. In contrast, rock units with relatively uniform strength profiles (i.e. similar degrees of weathering and fracturing at the surface and at depth) may produce deeper, larger landslides and have lower power-law exponents (Clarke & Burbank, 2010; Frattini & Crosta, 2013; Hurst et al., 2013)

Landslide erosional budgets also depend on the volumes of material mobilized (e.g. Larsen et al., 2010; Korup et al., 2012). For practical reasons, landslide volumes are often estimated from landslide areas, based on field-calibrated scaling relationships that take the form of a power-law (e.g. Guzzetti et al., 2009; Larsen et al., 2010):

$$V = \alpha A^{\gamma} \quad \text{(Equation 2)}$$

where *V* is the volume of a single landslide deposit, the landslide failure (scar) or both, depending on the study; *A* is the mapped area for that landslide; and α and γ are dimensionless scaling parameters which can vary depending on the setting and landslide type. Larsen et al. (2010) found that for bedrock landslides, where depths are limited by bedrock fracturing and rock strength (e.g. Clarke & Burbank, 2010), γ ranges between 1.3-1.6; while for shallow soil landslides, where depths are limited by soil thickness, γ has values of 1.1-1.4. The prevalence of these landslide types depend

This article is protected by copyright. All rights reserved.

on how soil formation rates compare to hillslope erosion rates (Larsen et al., 2010), which can be influenced by lithology. In contrast, Guzzetti et al. (2009) found that a single volume-area scaling relationship fitted reasonably well a mixed dataset of 677 landslides, suggesting that area-volume scaling is predominantly a geometrical effect. Overall, these studies show that lithology and rock strength can significantly affect landslide erosional dynamics, but their influence on slopes, landslide occurrence, frequency distributions and area-volume scaling have never, to our knowledge, been explored concomitantly for the same data set.

Grain size supply from hillslopes to channels: controls and impact on fluvial sediment

Theoretical (Sklar & Dietrich, 2004; Whipple & Tucker, 2002) and field data (Cowie et al., 2008) demonstrate that fluvial incision rates depend on the rates and grain sizes of sediment supplied to channels. Over short transport distances, where grain size distributions do not significantly change via abrasion and selective deposition, the calibre of fluvial sediment is determined by the grain size distributions supplied by the adjacent hillslopes (e.g. Ibbeken, 1983; Wolcott, 1988; Attal & Lavé, 2006; Sklar et al., 2006b; Mueller et al., 2016). However, the controls on grain size supply from hillslopes have received little attention until recently (Allen et al., 2015; Attal et al., 2015; Riebe et al., 2015; Sklar et al., 2016).

The grain size distributions of fluvial and hillslope sediment tend to follow exponential patterns similar to those of fragmentation processes (Krumbein and Tisdel, 1940; Wolcott, 1988; Ibbeken, 1983; Allen et al., 2015). Sources of sediment from hillslopes include rock falls, scree cones, landslides, soils and weathering of bedrock outcrops. Rock fall and landslide deposits have been found to be poorly sorted (with lithology and degree of fracturing of the parent rock exerting a primary control on their grain sizes (Hewitt, 1999; Casagli et al., 2003; Dunning et al., 2006; Attal and Lavé, 2006). Landslides have been found to deliver coarser grain size distributions than other sediment sources, and both bimodal and unimodal distributions have been reported (Casagli et al., 2003; Attal and Lavé, 2006; Whittaker et al., 2010; Attal et al., 2015). Consequently, sediment inputs from landslides have been found to coarsen fluvial sediment in landslide-prone reaches, and to generate bimodal grain size distributions

This article is protected by copyright. All rights reserved.

Accepted Article

and/or downstream coarsening (Ibbeken, 1983; Ibbeken & Schleyer, 1991; Attal and Lavé, 2006; Whittaker et al., 2010, Attal et al., 2015; Mueller, 2016; Sklar et al., 2016).

Recently, attention has focused on the grain size distributions of sediment supplied by soils and bedrock weathering, which are predicted to vary depending on lithology, climate, topography and erosion rates (Sklar et al., 2016). The limited empirical data available supports the existence of climatic and altitudinal controls (Marshall and Sklar, 2012; Riebe et al., 2016), hillslope gradient/residence time controls (Attal et al., 2015), and lithological controls (Allen et al., 2015) on the grain sizes supplied to channels. In soils, finer grain size distributions are produced in sectors of enhanced weathering, such as lower, warmer elevations, hillslope bottoms or north-facing slopes (Sklar et al., 2016); or low-gradient hillslopes where particles are potentially exposed for long periods to weathering processes that can reduce their grain sizes (Attal et al., 2015). The median grain size and the abundance of rock fragments in soils have been found to be correlated (Marshall and Sklar, 2012), and to increase with rock tensile strength (Sklar et al., 2016).

Overall, these studies suggest that the grain size distributions of sediment supplied from hillslopes are somewhat predictable (e.g. Sklar et al., 2016). The grain size distributions input to channels are expected to be coarser when they are supplied by landslides (e.g. Attal & Lavé, 2006; Whittaker et al., 2010; Attal et al., 2015), delivered from stronger rocks with low fracture density (e.g. Allen et al., 2015; Sklar et al., 2016), experience shorter weathering zone residence times (Attal et al., 2015; Sklar et al., 2016), and when physical weathering dominates over chemical weathering (Marshall & Sklar, 2012; Riebe et al., 2015; Sklar et al., 2016). However, empirical data evaluating how these variables affect grain size distributions is still limited, and systematic comparisons of grain size distributions supplied from different lithologies and processes are scarce. Open questions include the extent to which: (i) grain size distributions supplied from bedrock weathering vary with rock strength; (ii) grain size distributions change depending on if they are supplied by weathering or landsliding, and if this change depends on the style of landsliding or lithology; (iii) the varying sources of hillslope grain size supply affect the fluvial sediment export from catchments.

Here, we address these questions in a study area where climate and tectonics are well-known and relatively uniform; so lithology, rock strength and delivery process (weathering vs. landsliding) are the main variables controlling grain size. We compare grain size

This article is protected by copyright. All rights reserved.

Accepted Article

distributions from 32 bedrock weathering sites and 40 landslide deposits, on sandstones, granites, gneisses and schists, and carbonates, for which we also measured rock strength at 35 localities. Finally, we evaluate the impact of sediment supplied from hillslopes on fluvial sediment, by comparing the grain size distributions delivered by weathering products and landslides with those of the fluvial export from 26 catchments affected by different degrees of incision and landsliding.

GEOLOGIC SETTING

Our study area, in southern Italy, comprises 8 mountain ranges bounded by normal faults, three in the southern Apennines (the Diano, Monti della Maddalena and Agri faults, in Campania-Basilicata), and five in Calabria (the West Crati, East Crati, Serre, Cittanova and Armo faults) (Fig. 1). These faults initiated during the Upper Pliocene in the southern Apennines and the Middle Pleistocene in Calabria (Pattaca & Scandone, 2007; Faccenna et al., 2011; Roda-Boluda & Whittaker, 2016, 2017). Their maximum long-term throw rates (vertical component of slip rates) range between 0.6-1.4 mm yr^{-1}, and the relief on their footwalls is ~1000-1500 m, with some footwall blocks having up to 800 m of inherited, pre-faulting relief (e.g. Papanikolau & Roberts, 2007; Galli & Peronace, 2015; Roda-Boluda & Whittaker, 2016, 2017). The fault-bounded catchments are still adjusting to these throw rates, experiencing an upstream-migrating wave of fluvial incision (Roda-Boluda & Whittaker, 2016, 2017) that induces landsliding at the valley sides (Fig. 1). The study area has been affected by about twenty M> 6 earthquakes over the last 2 kyr, most recently in 1980 in the southern Apennines and in 1908 in Calabria (e.g. Galli & Peronace, 2015). The area has a Mediterranean climate with mountainous areas characterized by mean annual temperatures of ~12°C and mean annual precipitation ranging betweeen 1200-1600 mm (e.g. Terranova et al., 2009). Although landslide-prone topography and earthquakes are clearly driven by the active tectonics, some studies have found that intense rainfall or snowmelt can also trigger landslide events (Petrucci et al., 2009; Polemio & Petrucci, 2010).

In Campania-Basilicata (Fig. 1a), the footwall blocks of the faults are uplifting flysch sandstones, carbonates and some red chert. Flysch formations (Gorgoglione, Galestrino, Albidona and Monte Sierio formations) comprise sandstone units, with

This article is protected by copyright. All rights reserved.

Accepted Article

some minor interbedded pelitic, marly and calcareous units; while carbonate units encompass massive or poorly-stratified limestones and dolomites, cherty limestones, calcarenites, and minor marly and sandy beds (1:100000 Italian Geological Survey maps and reports, field observations). Sandstone and marl-clay complexes are more prone to landsliding than other lithologies (Santangelo et al., 2013; Coico et al., 2013). In Calabria, footwall bedrock is the Paleozoic crystalline basement composed of gneisses and schists with intruded granitoids (Fig. 1b and c; e.g. Fazio *et al.*, 2015). These rocks have variable degrees of weathering and can have alteration profiles up to ~50 m deep (Le Pera & Sorriso-Valvo, 2000; Borrelli et al., 2014; Scarciglia et al., 2016; Von Eynatten et al., 2016). Reported Schmidt hammer rebound values (a proxy for rock strength, see methods) for these crystalline rocks range between <10 to 50, with the higher values found in fresher and less fractured bedrock (Goswami et al., 2011; Borrelli et al., 2014; Scarciglia et al., 2016).

The Italian Geological Survey (ISPRA) has published a geomorphological landslide map (sensu Galli et al., 2008; Guzzetti et al., 2012) for Italy, under the IFFI project (Inventario dei Fenomeni Franosi in Italia; e.g. Trigila et al., 2010). This inventory was compiled by several teams and contains over 480,000 landslides identified using aerial imagery, field surveys, previous inventories and historical and archive data. Other landslide inventories in southern Italy focus on small areas (<120 km^2) and report high landslide densities, with landslides covering between 3-40% of the study areas (e.g. Conforti et al., 2011, 2014; Bianchini et al., 2012; Goswami et al., 2011; Santangelo et al., 2013). There is a large body of risk-oriented and monitoring landslide studies in southern Italy (e.g. Terranova et al., 2007; Bianchini et al., 2012; Giocoli et al., 2015), but few studies have evaluated landslides from a landscape evolution or sediment supply perspective (Lazzari & Schiattarella, 2010; Goswami et al., 2011, 2016; Santangelo, 2013; Antronico et al, 2015). Landslide frequency-area statistics have only been evaluated by Goswami et al. (2011) for <400 landslides in a small section of the Aspromonte massif (Calabria), and by Santangelo et al. (2013) for the Sinni River catchment in the southern Apennines. Goswami et al. (2011) found β=1.94; while the data from Santangelo et al. (2013) imply a β=2.16, not dissimilar to the exponent found by Guzzetti et al. (2002) in the central Apennines of β=2.5. Multi-temporal inventories spanning a few years or decades of activity imply landslide rates of between 3.3 to 1.4x10^{-4} landslides yr^{-1} km^{-2} (Petrucci & Polemio, 2000; Terranova et al., 2007; Petrucci et al., 2009; Polemio & Petrucci, 2010;

This article is protected by copyright. All rights reserved.

Accepted Article

Falconi et al., 2013; Polemio & Lonigro, 2013; Conforti et al., 2014; Antronico et al., 2015; Goswami et al., 2016), although these inventories may be biased towards large, damaging events. A few of these studies provide estimates of landslide-related catchment erosion rates: 0.46 mm yr^{-1} (Lazzari & Schiattarella), 0.26 mm/yr (Antronico et al., 2015), and 2.8-3.4 mm yr^{-1}, albeit for a short time period (Goswami et al., 2016). Cosmogenic nuclide-derived catchment erosion rates in Calabria are 0.1–1 mm yr^{-1}, with a mean value of ~0.5 mm yr^{-1} (Cyr et al., 2010; Olivetti et al., 2012; Roda-Boluda et al., 2017); while for the Southern Apennines, ^{10}Be erosion rates and volumetric erosion estimates are ~0.1-0.5 mm yr^{-1}, with a mean value of ~0.3 mm yr^{-1} (Amato et al., 2003; Lazzari & Schiattarella, 2010; Gioia et al., 2011; Roda-Boluda et al., 2017). Therefore, landslide-related erosion rates are comparable in magnitude to catchment-averaged erosion rates (and fault throw rates), which implies that landslides are a major source of hillslope sediment supply in the area.

METHODS

Fault maps for all normal faults are taken from Roda-Boluda & Whittaker (2016, 2017). Lithologies were determined from the digital Italian Geological Survey (ISPRA) lithological map; and checked in the field. Topographic data were derived from the ASTER digital elevation model (DEM), with a resolution of 27.3 x 27.3 m. A total of 152 footwall catchments with areas >2.5 km^2 were extracted upstream of the studied faults, and were assigned a dominant lithology when a lithological group covered ≥50% of the catchment area; otherwise, they were classified as having mixed lithologies. Slope maps (included in the supplementary material) were derived from the DEM, and the mean slope for each catchment, and relative frequency of slopes for each of the main lithologies, were extracted from these slope maps. Because the studied catchments have different amounts of inherited, pre-faulting relief, catchment incision, which has propagated from the faults as knickpoints migrate upstream, is a more representative metric of catchment geomorphology in the landslide-prone areas (which are typically downstream of knickpoints) than relief (Fig. 1, see slope and incision maps, and comparisons of relief and incision in the supplementary material). For each pixel in the DEM, incision depth was calculated as the maximum vertical distance between the drainage divide and the valley bottom; the maximum value for each catchment represents catchment maximum incision depth. This was derived by

This article is protected by copyright. All rights reserved.

Accepted Article

creating a TIN surface capping the catchment around the drainage divide and subtracting the clipped catchment DEM from this surface (see supplementary material). In Fig. 2, we present this data as incision normalized by catchment area to account for the fact that larger catchments tend to have greater incision depths (see supplementary material). Subsequent calculations and data analysis have been performed in ArcGIS v.10.3 and OriginLab Pro 2017. For plots with errors on the x-axis, we used the York least squares regression method (York, 1968), rather than the ordinary least squares (OSL) one. Errors on the regressions are standard errors on the parameter estimates, reported R^2 values are *adjusted* R^2, and the reported *p* values are for the *t-test* (Prob>|t|).

Landslides

For our geomorphological inventory, we focused on landslides within the fault-bounded catchments or within two kilometres of the faults, where most landslide-prone hillslopes are located. We digitized the landslides mapped by the IFFI project within these boundaries (2470 landslides), and identified recent landslides in Google Earth imagery acquired between 2002 and 2014 at a 15 m resolution (319 landslides). Recent landslides were identified following the criteria outlined by Guzzetti et al. (2012); identifying landslide scars and deposits by their shapes, changes in terrain roughness, colour, vegetation cover, and their topographic settings (generally high-angle hillslopes). These inventories were checked during two field campaigns in 2013 and 2014. The separate inventories and examples of landslides mapped in Google Earth can be found in the supplementary material. The IFFI project map categorizes landside types; however, we found in the field that, likely because different areas were mapped by different teams, this classification was not always consistent. Consequently, we chose not to differentiate landslide types in this study. We divided the landslide inventory based on the affected lithology, for the four major bedrock lithologies in the area: carbonates, flysch sandstones, granites, and gneisses and schists.

We calculated the frequency density of landslide sizes by applying Eq. 1 for the non-cumulative number of landslides. Following other authors (Malamud et al., 2004; Van Den Eeckhaut et al., 2007; Hurst et al., 2013), we use bins of equal logarithmic width,

This article is protected by copyright. All rights reserved.

so that the linear width of the bins (w) increases with A_L ($w_i = A_{Li+1} - A_{Li} = A_{Li}(10^b - 1)$, with b being an arbitrary fixed exponent, 0.1 in our case, which best reflects our data (White et al., 2008; Huang et al., 2014). We normalize N_L by bin width, obtaining a non-cumulative frequency density. Logarithmic binning has the advantage of reducing the number of zero and low count bins at large areas, while the normalization reduces the biases and cumulative effect caused by the increasing bin widths. We obtain the non-cumulative power law negative exponent, β, by fitting a power-law for the landslides between the rollover and the maximum A_L value. Catchments landslide densities were calculated as the ratio of the total area covered by landslides and catchment area. Lithological landslide enhancement factors (L_{EF}) were calculated for each lithology as (i.e. Borgomeo et al., 2014):

$$L_{EF} = \frac{A_{LL}/A_{LT}}{A_{Lit}/A_T} \quad \text{(Equation 3)}$$

Where A_{LL} is the area covered by landslides in each lithology, A_{LT} is the total area covered by landslides in the study area, A_{Lit} is the outcropping area of each lithology, and A_T is the total study area (catchment area plus a 2 km band along the studied faults). A L_{EF} value of 1 indicates that landslide occurrence mirrors the areal abundance of a lithology; $L_{EF}<1$ indicates that landslides are underrepresented in that lithology, and $L_{EF}>1$ that they are overrepresented.

In the field, we estimated the dimensions of 8 landslide deposits using a laser range finder, to derive a local area-volume relationship. Depending on landslide geometry, volumes were estimated using the volume equation for a cuboid or for a half-cone. We added to our calibration the large Verdesca landslide, at the tip of the Agri fault (Fig. 1a) whose thickness has been estimated with electrical resistivity tomography and boreholes as varying between 10 to 30 m (Giocoli et al., 2015); we use a value of 15 m, half the maximum, as a depth approximation. Sampled landslides span the four major lithologies in the area (sandstones, carbonates, granites, and gneiss and schists), and have soil and fine sediment (<1 mm) content ranging from 15-70% (a proxy for bedrock-soil components of landslide type). Landslide depth was calculated by dividing volume by area (e.g. Guzzetti et al., 2009), and accounting for landslide

This article is protected by copyright. All rights reserved.

bulking due to dilation, of a factor of ~2 for the range of landslide sizes that dominate our inventory (according to the landslide deposit–to-scour ratios suggested by Larsen et al., 2010, in their supplementary material). Sediment flux from landslides is dependent on the rate of landsliding, which is not known for our geomorphological inventory. However, we exploit a simple equation proposed by Malamud et al. (2004b):

$$\bar{e}_L = \frac{V_{LT}}{A_T T_L} \quad \text{(Equation 4)}$$

where V_{LT} is the total volume of landslides in the inventory, A_T the total area over which landslides have been mapped, and T_L the time over which the landslides have accumulated. T_L is unknown but plausible values of $\bar{e}_L$ can be approximated based on published catchment-averaged erosion rates. Therefore, we use Eq. (4) to estimate T_L and minimum landslide rates from our inventory.

Rock strength and grain size

We characterized outcrop-scale rock strength at 35 localities across all studied lithologies using a Schmidt hammer. Although the Schmidt hammer was originally designed to be a measure of a material's intact strength, several studies have found that it can be useful to characterise the degree of fracturing and weathering of rocks (e.g. Selby et al., 1980, 1982; Goudie, 2006; Borrelli et al., 2014), and we exploit this. The Schmidt hammer rebound test provides dimensionless values between 0 and 100 that are greater for less weathered and less fractured rocks, and that correlate with the uniaxial compressive stress of the rock (e.g. Selby et al., 1980; Aydin & Basu, 2005; Minaeian & Ahangari, 2013). Following other authors (e.g. Aydin & Basu, 2005) we took 10 Schmidt hammer measurements perpendicular to the bedrock surface. We obtained these readings in multiple representative parts of the outcrop, not favouring unweathered or unjointed sectors, because the goal was to characterise the actual strength of the bedrock outcrop including weathering and fracturing, not an approximation of intact strength. However, because each Schmidt hammer rebound test only characterises the elastic response of a limited volume of rock around the test site, the Schmidt hammer measurements do not account for fracturing at greater scales, or for other variables such as fracture orientation, persistence or width, which

This article is protected by copyright. All rights reserved.

may significantly impact rock mass strength at hillslope scales (e.g. Selby et al., 1980, 1982; Moore et al., 2009; Clarke & Burbank, 2010). For each locality, we calculated the mean and standard error from 10 measured values; and from these, the mean and standard error of the Schmidt hammer rebound values for each lithology. We complemented our data set with Schmidt hammer data from Borrelli et al. (2014) (see supplementary material).

In 32 of these bedrock outcrop localities, we also measured the grain size distribution of the bedrock weathering products, for grains ≥1 mm, using the Wolman point count method (Wolman, 1954). Twenty-six of the grain size distributions were counted in the field, and 6 were obtained by counting on high-resolution, scaled photographs, which produces distributions statistically indistinguishable from field measurements (Casagli et al., 2003; Cowie et al., 2008; Whittaker et al., 2010, 2011; see supplementary material). Using the same method, we measured the grain size distributions of landslide deposits at their surface for 40 localities. In each locality, care was taken to sample representative areas, and grain sizes were measured across several m^2. Although mobilization of material during landsliding may result in sediment sorting across the deposit (e.g. Casagli et al., 2003; Dunning et al., 2006), the choice of sampling localities was limited by accessibility in many cases. In 4 large landslides, we could sample in 2 or 3 separate localities across the landslide deposit. In order to compare sediment input from hillslopes with that being exported from the catchments, we also measured in the field the grain size distributions of fluvial sediment at the outlets of 26 catchments with landslide densities >2%, along the Agri, East Crati, Cittanova and Armo normal faults. We did Wolman point counts across several meter-squared patches of the surfaces of both channels and fluvial bars, which due to vertical sorting could reflect systematically coarser distributions than subsurface grain size (Attal & Lavé, 2006). From the grain size distributions, we extracted the median, D_{50} (50^{th} percentile) and the coarse-fraction, D_{84} (84^{th} percentile). We also combined, for each lithology, all the grain size measurements of each sediment type (weathering, landslide and fluvial), and use these to build amalgamated probability density functions of grain size using 2 mm bins.

Although Wolman point counting (Wolman, 1954) has the advantage of being a very time-efficient technique, errors on D_{50} and D_{84} are hard to determine. Due to vertical and lateral sorting within the deposits, repeat counts in different sites of the deposit

This article is protected by copyright. All rights reserved.

may not necessarily be similar. Additionally, grain size counts are potentially subjective and different people may be biased towards particular shapes or sizes (Buscombe, 2008; Whittaker et al., 2010). Therefore, we do not unrealistically attribute a specific error to each D_{50} and D_{84} values. However, repeat measurements by different people on the same few m^2 spots reveal that absolute errors for D_{50} range between 3-5 mm, with a mean of 3 mm; and for D_{84}, between 3-11 mm, with a mean of 7 mm (see supplementary material). This translates into relative errors of between 6-20% for D_{50}, with a mean of 12%, and between 7-26% for D_{84}, with a mean of 13%. These error ranges are likely applicable to all our grain size distributions, and are very similar to those found in grain size counts by Whittaker et al. (2011). Moreover, Wolman point counting has the disadvantage of not capturing the full grain size distribution (in our case, particles <1 mm). The concentration of fine sediment and suspended-bedload partitioning are important variables, affecting for example channel slopes and incision (e.g. Lamb et al., 2008), but they are hard to constrain (Turowski et al., 2010). Sieved grain sizes from 19 catchments in eastern Calabria, with similar relief, area and lithology to ours, show that sand content (<2 mm) of the bedrock weathering products ranges between 0-9%, with an average of 4%; and on fluvial sediment measured just downstream of the faults (like in our case), between 7-28%, with an average of 17% (Ibbeken, 1983; Ibbeken & Schleyer, 1991). Therefore, our Wolman point count data is most likely representative of >70% of the total fluvial sediment fluxes, and of >90% of the bedrock weathering grain sizes. The fine fraction on landslides is more variable, with lanslides in the central and northern Apennines, in carbonates and sandstone and calcareous flysch, having from 10% to 80% of material <2 mm (Casagli et al., 2003; Whittaker et al., 2010). This range agrees with our field observations (Table 2) of between 15-70% of landslide material <1 mm, but given that we could only sample landslide surfaces, where the suspended load fraction has likely been preferentially washed away, these should be considered minimum estimates, and we only focus on characterising the grain size distributions of the >1 mm fraction.

Accepted Article

This article is protected by copyright. All rights reserved.

RESULTS

Lithologic controls on sediment flux from landslides

A total of 2789 landslides were recognised in our study region of 2600 km^2, with areas between 213 m^2 and $3.7x10^6$ m^2. Landslides are found along the incised fluvial valleys, or along the fault traces, sometimes affecting the Pleistocene deposits exposed at the proximal hanging-wall basins (Fig. 1). Landslides cover between 0.05-73% of the areas of affected catchments, and overall landslide density in the study area is 8.7%.

Slopes

The abundance of steep slopes (>20º) is one of the main factors that influences landslide activity. In the study area, steep slopes are associated with the tectonically-controlled fluvial incision (Fig. 1, see supplementary material for slope and incision maps), which has propagated through the catchments as knickpoints migrate upstream from the faults (Roda-Boluda & Whittaker, 2016, 2017). Hence, catchment mean slopes are expected to increase as incision deepens, until they reach a limit that is a function of hillslope equilibrium angles. Fig. 2a shows that as incision increases (presented as area-normalized incision, see methods), catchment mean slopes appear to reach an upper limit at around 23º. Assuming that downstream of knickpoints erosion rates match incision rates (which is the case for our study area; Roda-Boluda, 2017: Roda-Boluda et al., 2017), this would imply that some hillslopes downstream of knickpoints have reached their threshold angles (see Fig. S6 in the supplementary material), and that in some areas of the catchments, further hillslope adjustments to continued incision occur by increasing the frequency of landsliding. Modal slopes in this area are relatively low (5-17º, Fig. 2b), because catchments are experiencing a transient response to tectonics and in some cases have low-slope upstream sectors still completely unincised (Fig. 1, see slope maps on the supplementary information; Roda-Boluda and Whittaker, 2016, 2017). Therefore, slope distributions cannot be interpreted in the same way as in steady-state landscapes (e.g. Montgomery, 2001), but they can still be informative about lithological differences. Slope distributions reveal significant differences across lithologies in the abundance of steep slopes, which could potentially influence landslide occurrence: slopes >20º represent 35% of carbonate slopes and 43% of gneiss slopes, but only 17% and 22% of sandstone and granitic

This article is protected by copyright. All rights reserved.

ones, respectively. Slopes >30º represent 10% of carbonate slopes, 12% of gneiss slopes, 8% of granitic slopes, and only 2% of sandstone slopes.

Landslide occurrence

Figure 3a shows that the proportion of area affected by landslides in each lithology is variable, with landslides affecting ~5% of granites and carbonates, but up to ~20% of the flysch sandstones. We convert these data into lithology enhancement factors (L_{EF}) using Eq. 3 (Fig. 3b). Landslide occurrence in the gneisses and schists (L_{EF}=0.86) approximately mirrors their outcropping area, whereas landslides on granites (L_{EF}=0.28) and carbonates (L_{EF}=0.54) are under-represented with respect to their outcrop areas. Landslides in sandstones are twice as likely to occur as it would be expected by their areal extent (L_{EF}=2.19), and are also over-represented in red chert (L_{EF}=1.35) and Pleistocene deposits (L_{EF}=1.53). Rock types with lower mean Schmidt hammer rebound values (weaker, more weathered and/or more fractured; Table 1) broadly tend to have greater L_{EF} values and hence are more prone to landsliding, while those with greater rebound values (stronger, less weathered and/or less fractured) have lower L_{EF}, and are therefore less susceptible to landsliding (Fig. 3c). The data falls into two distinct groups: lithologies with mean Schmidt hammer values <20 have L_{EF}>1 while those with Schmidt hammer values >20 have L_{EF}<1.

Landslide frequency-area distribution

The overall cumulative distribution of landslides (Fig. 4a, black line) shows that the median size of landslides in the inventory is 0.025 km^2, 80% of them are <0.06 km^2 and 85% <0.1 km^2. However, there are lithological differences: median-sized landslides for the granites are 0.012 km^2, while those in sandstones are 0.037 km^2. Likewise, landslides <0.1 km^2 represent 92% of those affecting granites, a greater proportion than for the overall inventory. The biggest landslide affecting each lithology is 2.0-3.7 km^2, and the smallest, on the order of 10^{-4} km^2. The similarity of these values suggests that the differences between lithologies in Fig. 4a are not simply due to differences in mapping resolution. The frequency density of the landslide inventory has a “rollover” at 0.02–0.04 km^2, for landslides where 0.04 km^2< A_L<3.7 km^2, the exponent of the power-law defining the frequency density is β=2.3±0.1, implying that the landslide inventory is not dominated by large landslides (Fig. 4b). Moreover, the relative contribution of landslides smaller than 0.02–0.04 km^2 is probably under-

This article is protected by copyright. All rights reserved.

represented in our geomorphological inventory. Whereas the overall distribution of landslide sizes is influenced by lithology (Fig. 4a), the rate of frequency decay of bigger landslides with respect to smaller ones (i.e. the rollover positions and power-law exponents) is similar for all lithologies (Fig. 4b).

Landslide area-volume scaling

We calibrate a landslide volume-area scaling relationship based on field estimates of 8 landslide deposits spanning all major lithologies and the soil-bedrock landslide spectrum (Table 2), and the volume of one landslide imaged by electrical tomography (Giocoli et al., 2015). The correlation follows a power law (Fig. 5a):

$$V = 0.253(\pm 0.028)A^{1.284(\pm 0.009)} \qquad \text{(Equation 5)}$$

Where area (A) is in m^2 and volume (V) is in m^3. This scaling is similar to those suggested by Guzzetti et al. (2009) and the global and bedrock scalings from Larsen et al. (2010), although for our study area both their scalings underestimate landslide volumes for small landslides and overestimate them for bigger landslides (Fig. 5b). Based on our scaling relationship, the median-sized landslides of the study area, with A=0.025 km^2, have a scar excavation depth of ~2.3 m; and the 85% of landslides that are <0.1 km^2 excavate to depths of about ~3 m. We can use Eq. 5 to estimate the total landslide volumes stored in the catchments, which are up to $1.5x10^8$ m^3 and have mean and median values of $8.1x10^6$ m^3 and $2.1x10^6$ m^3, respectively. These volumes, V_{LC}, can be normalized by catchment area, A_C, to account for the fact that bigger catchments tend to have more landslides; the normalized volumes represent the thickness of landslide deposits if these were spread uniformly across the whole catchment area. These thicknesses (V_{LC}/A_C) typically reach values of 0.2-2 m, with a mean and median value of 0.7 m and 0.3 m respectively.

Inventory timescale and landslide rates

We lack information about the time of landslide accumulation that our landslide inventory represents, and hence landslide rates. We use Eq. 4 to estimate plausible inventory timescales, T_L, using the median and mean V_{LC}/A_C values for the catchments (above), and an overall V_{LT}/A_T value calculated using the total volume of landslides stored in all catchments and catchments total area, including those that currently have no landslides. T_L decreases with increasing landslide-related erosion rate, $\bar{e}_L$, which is

This article is protected by copyright. All rights reserved.

unknown but can be approximated from published catchment-averaged erosion rates (Fig. 6a). Although Eq. 4 assumes that all sediment flux is derived from landslides (which may be appropriate for the study area; Lazzari & Schiattarella, 2010; Goswami et al., 2016; Roda-Boluda, 2017; Roda-Boluda et al., 2017), we use a wide range of erosion rate values to cover most plausible landslide erosion scenarios in these first-order calculations. Given the erosion rates reported in the area (Fig. 6a, inset), a plausible maximum $\bar{e}_L$ value is ~0.5 mm yr^{-1} (the maximum and mean erosion rate in the Southern Apennines and Calabria, respectively), while a plausible minimum $\bar{e}_L$ is ~0.15 mm yr^{-1} (50% of the mean erosion rates in the southern Apennines). With $\bar{e}_L$~0.5 mm yr^{-1}, our inventory would represent landslide accumulation over 1 kyr; while if $\bar{e}_L$~0.15 mm/yr, T_L~3 kyrs. With $\bar{e}_L$<0.1 mm yr^{-1}, T_L rapidly increases (Fig. 6a, inset), but such low erosion rates have only been measured in the unincised regions of catchments, where there are no records of landslide activity (Olivetti et al., 2012; Roda-Boluda, 2017). If our inventory plausibly represents landsliding over the last ~1-3 kyr, then based on the number of landslides and catchment areas, minimum landslide rates, L_R, would be of the order of 10^{-4}-10^{-3} landslides yr^{-1} km^{-2}, with mean values of L_R~$1x10^{-3}$ landslides yr^{-1} km^{-2} when T_L= 1 kyr, and mean L_R~$4x10^{-4}$ landslides yr^{-1} km^{-2} if T_L=3 kyr. These values are all minima because geomorphological landslide inventories represent the integrated record of landslide supply and removal, not a complete record of landsliding.

Grain size supply from hillslopes: lithologic and process controls and effects on fluvial sediment export.

Lithologic controls on bedrock weathering products

In the field, we measured the grain size distributions supplied by bedrock outcrops (Fig. 7a and b, Table 1) and by landslides (Fig.7c and d, Table 3). We find that the grain sizes supplied from bedrock outcrops correlate with Schmidt hammer rebound value, with both D_{84} and D_{50} values increasing ~10 mm for each 10-point Schmidt hammer rebound value increment, and doubling from over a 40-point Schmidt hammer value increase (Fig. 8). The correlation of D_{50} values with Schmidt hammer rebound is weaker (Fig. 8b, R^2=0.25 vs. R^2=0.48 for D_{84}), suggesting that rock strength has more control over the coarse-fraction of bedrock grain size supply. However, the trend

This article is protected by copyright. All rights reserved.

seems to be dominated by the carbonates and granites; while sandstones and gneisses and schists seem to have more uniform grain sizes, perhaps due to their more pervasive fabrics.

Process controls: bedrock weathering vs. landslides

Landslides are expected to supply coarser grain sizes than bedrock weathering, but the degree of coarsening with respect to weathering products has not previously been quantified across different lithologies. We compare the grain sizes supplied by landslides and bedrock weathering for sandstones (Fig. 9a), gneisses and schists (Fig. 9c), granites (Fig. 9d) and carbonates (Fig. 9b). For the first three lithologic groups, landslides tend to supply overall coarser sediment, although a few landslides supply material with similar distributions to the bedrock weathering products. In contrast, for carbonates, the grain sizes supplied by bedrock weathering and landslides are indistinguishable (Fig. 9b). We hypothesize that the distributions are most similar when most of the landslide material is inherited from the top soil and weathered profiles. Comparison of the grain sizes obtained in different localities of the same landslide (9 localities in 4 landslides) reveal that in two cases, the differences in D_{50} and D_{84} values obtained in distal localities of the landslide deposit are <15% (within the range of uncertainty, see methods) while the other two landslides exhibit 20-60% differences between sampling localities, probably due to grain size sorting within the landslide deposit (Table 3).

We summarize these grain size data in Figs. 9e and 9f, presenting in box plots the D_{84} and D_{50} values of all bedrock weathering and landslide distributions for each lithology (Tables 1 and 3). Landslides in sandstones supply 40-60% coarser grain size distributions than the products of sandstone weathering, with a median D_{84} of 66 mm, while landslides in gneiss supply median D_{84} values of 80 mm, 20-30% coarser than gneiss weathering products. Only one landslide could be sampled that eroded granite, but this supplied a D_{84} of 97 mm, ~250% coarser than for bedrock weathering, showing a major difference. Figures 9e and 9f confirm that bedrock weathering and landslides in carbonates supply similar grain sizes, with median D_{84} values of 55 mm and landslides supplying only 5-15% coarser material. For all lithologies, average D_{50} values supplied by landslides fall in a relatively narrow range of 28-34 mm, while D_{84} values are more variable.

This article is protected by copyright. All rights reserved.

Accepted Article

Effects on fluvial sediment export

Owing to the generally coarser landslide supply (Fig. 9) catchments affected by more landsliding should be expected to export coarser grains sizes to the adjacent basins. Whereas current landslides in each catchment could be greatly influenced by recent landslide activity and degree of preservation of their deposits, more incised catchments are expected to have greater long-term rates of landsliding. We observe that catchments with greater incision depth, d_i, deliver coarser grain sizes, across all sampled lithologies (Table 4, Fig. 10a and b). The differences are more significant in the coarse fraction (D_{84}), which almost doubles in size over a 500 m increase in d_i (Fig. 10a), at a rate of ~10 mm for each 100 m increment in incision depth. To test if coarsening in sediment export is only due to differences in effective discharge between the catchments, D_{84} and D_{50} are plotted against catchment drainage area, A, since data from Ferro & Porto (2012) demonstrate that discharge scales almost linearly with catchment area in southern Italy (Figs. 10c and d). The correlation of grain size with catchment area (i.e. discharge) is considerably weaker (comparing R^2 and *p-values*) than with incision, so we hypothesize that the linear scaling of grain size with d_i reflects enhanced landslide supply in addition to greater transport capacity in more incised catchments.

We summarize our grain size data by comparing the relative frequencies of grain size fractions of bedrock weathering, landslide supply, and fluvial sediment export, for each lithology, built from the amalgamated grain size distributions of all localities in each category (Fig. 11). Overall, the modalities of fluvial export relative frequency curves are very similar to the modalities of weathering and landslides supply (e.g. Fig. 11a and c), or fall in between these two input pdfs (e.g. Fig. 11d), but the frequency distributions of fluvial export are slightly enriched in coarser grains.

DISCUSSION

Landsliding in southern Italy and comparison with previous inventories

Our inventory reveals an overall areal density of landslides of 8.7%, and catchment landslide densities of up to 73% (Fig. 1), comparable to reported landslide densities in

This article is protected by copyright. All rights reserved.

Accepted Article

southern and central Italy (3-40%; e.g. Guzzetti et al., 2002; Conforti et al., 2011, 2014; Bianchini et al., 2012; Santangelo et al., 2013; Borgomeo et al., 2014). Our inventory resolution (given by the smallest landslide mapped and the rollover value of the frequency density) and power-law exponent are also similar to other inventories in southern and central Italy (e.g. Guzzetti et al., 2002; Santangelo et al., 2013; Borgomeo et al., 2014). The size of the largest landslide in our inventory, 3.7 km^2 (Fig. 4), is consistent with those reported in central and southern Italy (4.1 km^2, Santangelo et al., 2013; 4 km^2, Guzzetti et al.,2012), suggesting that this may be the upper limit of landslide sizes in the region, restricted by hillslope lengths and bedrock fracturing (e.g. Clarke & Burbank, 2010; Frattini & Crosta, 2013). Our data confirms that landsliding in this area is dominated by medium and small landslides (the latter probably being more relevant than can be inferred from these geomorphological inventories), which is also supported by the observations that 50% of the landslides are <0.0025 km^2 and 85% are smaller than 0.1 km^2 (Fig. 4a).

We present the first field-calibrated area-volume scaling for landslides in southern Italy (Fig. 5a), from which we estimate that 50% and 85% of landslides excavate to depths of ~2.3 m and ~3 m respectively, enabling us to quantify the observations made by many authors that landslides in the area are generally shallow (Calcaterra & Parise, 2005, 2010; Goswami et al., 2011; Conforti et al., 2011). These results are similar to observations by Guzzetti et al. (2009) that the average landslide depth in the central Apennines is 2.7 m. The area-volume power law exponent, γ=1.28, falls in the range where Larsen et al. (2010) found that the exponent values of soil (γ=1.1-1.4) and bedrock (γ=1.3-1.6) landslides overlap. Given that our scaling relationship fits across the spectrum of sampled landslides, ranging from soil to bedrock landslides, and affecting all major lithologies in the area (Table 2), this suggests that the excavation depths of the sampled soil and bedrock landslides are not substantially different in our study area. This similarity is probably because in the study area, the reported soil depths and the depths of weathered and fractured profiles that generate bedrock landslides, are comparable (e.g. Calcaterra & Parise, 2005, 2010; Borrelli et al., 2014; Scarciglia et al., 2016). The relative contributions of soil (i.e. shallow) and bedrock (i.e. deep) landslides to the inventories depend on how soil formation rates compare to hillslope erosion rates (Larsen et al., 2010), and on the rock strength gradient with depth (e.g. Clarke & Burbank, 2010; Frattini & Crosta, 2013). Landsliding is characterized by bedrock failures where soil

This article is protected by copyright. All rights reserved.

Accepted Article

formation rates lag behind hillslope erosion rates and/or bedrock rock strength is uniform with depth. While the depth profile of bedrock cohesion and fracturing is hard to estimate, soil and weathering profile formation rates have been recently estimated in the Sila massif (Fig. 1) by Scarciglia et al. (2016) to be between 0.01-0.36 mm yr^{-1}. Therefore, the rates at which weathering profiles and soils develop can be of the same order of magnitude as catchment-averaged erosion rates, of 0.1–1.0 mm/yr (Lazzari and Schiattarella, 2010; Cyr et al., 2010; Olivetti et al., 2012; Roda-Boluda, 2017). The fact that weathering and soil formation rates do not lag much behind catchment erosion rates could explain why our volume-area scaling exponent falls on the upper end of soil landslide exponents, and on the lower end of bedrock landslide exponents.

The thickness of mobilized landslide material in the catchments, with typical values of ~0.3-0.7 m, compares well with those found in the central Apennines by Guzzetti et al. (2009) of 0.46 m. Minimum landsliding rates inferred from our inventory, of 10^{-3}-10^{-4} landslides yr^{-1} km^{-2} are lower than the typical values of multi-temporal inventories in the area, with a mean of $3.8x10^{-1}$ landslides yr^{-1} km^{-2} and a median of $6.4x10^{-3}$ landslides yr^{-1} km^{-2} (Fig. 6b, see geological setting and Table S1), likely because these studies characterize landsliding over a few years to decades, while our geomorphological inventory captures the integrated record of landslide supply and removal over timescales that we estimate to be ~ 1-3 kyr (Fig. 6a). Overall, our data shows that landslides in the area probably mobilize volumes of material that can have a substantial impact on catchment erosion and basin stratigraphy, highlighting the importance of evaluating (i) how lithology modulates landslide fluxes, and (ii) the impact of landslides on hillslope grain size supply.

Lithological controls on hillslope sediment supply

Landslide activity

Our data suggest that lithology and rock strength modulate hillslope sediment fluxes by influencing slopes, landslide abundance, and the distribution of landslide sizes. Most catchment mean slopes are <23º; which, if representative of threshold slopes, is a lower angle that in other areas, probably due to the high degree of bedrock weathering and fracturing in the study area (Le Pera & Sorriso-Valvo, 2000; Borrelli et al., 2014; Scarciglia et al., 2016; Von Eynatten et al., 2016), and the preservation of unincised sectors

This article is protected by copyright. All rights reserved.

Accepted Article

upstream of knickpoints (Roda-Boluda & Whittaker, 2016, 2017). Rock strength has been reported to influence slope distributions (Korup, 2008; Korup & Schlunegger, 2009; Clarke & Burbank, 2010); in our area, we find that stronger rocks (carbonates and gneisses and schists) have greater proportions of steep slopes (>20º) than the weaker rocks (sandstones and granites) (Fig. 2b).

Similarly to other settings (Korup & Schluengger, 2009; Clarke & Burbank, 2010; Hurst et al., 2013; Borgomeo et al., 2014), we find at a regional scale that weaker rocks are more prone to landsliding, and we quantify this effect by combining Schmidt hammer measurements with our landslide inventory (Fig. 3), confirming that landslides in southern Italy are more widespread in weak flysch sandstones (Carrara et al., 1977; Santangelo et al., 2013; Coico et al., 2013; Conforti et al., 2014). Granites have a lower L_{EF} than could be expected by their rock strength (Fig. 3c), which could be due to the fact that landslides affecting granites are considerably smaller than those affecting other lithologies, and are therefore preferentially under-sampled (Fig. 4). Indeed, field observations have pointed out that landslides affecting granites are tightly coupled to the weathering profiles, and hence tend to be small and shallow (e.g. Calcaterra & Parise, 2005, 2010; Borrelli et al., 2014).

Although lithology influences the overall distribution of landslide sizes when the full spectrum of sizes is considered (Fig. 4a), it seems to play a minor role when only the decay in frequency of larger landslides is taken into account (Fig. 4b). This discrepancy could reflect that the two factors that control landslide sizes; (i) rock strength gradient with depth (Clarke & Burbank, 2010; Frattini & Crosta, 2013), and (ii) the ratio of soil production and erosion rates (Larsen et al., 2010), are significantly influenced by lithology for smaller landslide sizes; while local relief and incision, which are dictated by tectonics, are more important than lithology in determining the occurrence of larger landslides. These results also highlight that when the frequency distributions of landslides are compared for different lithologies, landslides below the rollover value of the distributions should also be considered. Our data set is too small to fully explore the influence of lithology on landslide area-volume scaling, but we note that all our data points, which include four lithologies, fall in the same trend, as found by Guzzetti et al. (2009).

Accepted Article

This article is protected by copyright. All rights reserved.

Grain size supply

Our data reveal that lithology and rock strength also control the grain sizes supplied from hillslopes, in two ways. First, rocks with greater rock strength tend to weather into coarser grain sizes (Fig. 8). Second, landslides, whose occurrence is controlled by lithology and rock strength (Fig. 3), deliver coarser grain size distributions than other erosional processes (Fig. 9). Moreover the grain sizes and degree of coarsening of landslides also varies across lithologic types (Figs. 9 and 11). This is the first time, to our knowledge, that the prediction of stronger rocks delivering coarser grain sizes (e.g. Allen et al., 2015; Sklar et al., 2016) is shown with empirical data from bedrock outcrops. We attribute this correlation to the fact that both the degree of weathering and fracturing at the outcrop scale are well-captured by Schmidt hammer rebound measurements (e.g. Selby et al., 1980, 1982; Goudie, 2006; Borrelli et al., 2014), and these two variables have a strong control on grain size production (Attal et al., 2015; Sklar et al., 2016). Rock- strength seems to have a stronger control over the coarse grain size fraction, D_{84}, probably because this is the fraction more closely related to fracture spacing. However, our results also highlight that rock strength and grain size supply can vary significantly within one lithologic group, depending on the local degree of weathering and fracturing, and that rock strength alone does not explain the observed grain size differences (Fig. 8). The variability in rock strength and grain size that cannot be attributed to lithology is probably due to differences in local climatic conditions and vegetation (mostly due to the altitudinal gradient), distance from the fault, or the local deformation history of each formation (e.g. Sklar et al., 2016). Our data set was collected to test the role of lithology and does not allow us to explore these other variables further, but this remaining variability should be the object of future work. Overall, our results demonstrate that rock strength does not only influence the evolution of grain size distributions by modulating abrasion rates (e.g. Sklar & Dietrich, 2001; Attal & Lavé, 2006, 2009; O'Connor et al., 2014), but it is also key in determining the initial grain size distributions supplied from bedrock weathering.

Moreover, our data reveal that lithology plays a role in the degree of coarsening with respect to bedrock weathering products, which ranges between 5-250%. This difference in grain sizes supplied from landslides and weathering is significantly smaller than the order of magnitude difference found by Attal et al. (2015) in northern California, probably because we sampled comparatively fresh weathering products of

This article is protected by copyright. All rights reserved.

Accepted Article

bedrock outcrops, while they sampled particles embedded on soils, which had been subjected to considerable subsequent weathering. The degree of coarsening between bedrock and landside products may be indirectly related to the style of landsliding and landslide excavation depth that is more characteristic for each lithology, and the degree of fracturing during landslide mobilization (e.g. Zhao et al., 2017), for which we have limited data. However, field observations suggest that landslides only occur in carbonates (the strongest lithology in the area, Fig. 3) where meter-scale soil or weathering profiles have been developed. If landslides in carbonates generally only mobilize the top soil or weathering profiles, this would explain why the grain size distributions of weathering products and landslides are indistinguishable. This could also be the case for some landslides in other lithologies which have similar distributions to their bedrock weathering products (Fig. 9). Our landslide grain size distributions have a similar range of magnitudes to those previously reported (e.g. Ibbeken , 1983; Attal & Lavé, 2006; Dunning, 2006; Whittaker et al., 2010) but are finer than other published distributions (e.g. Casagli et al., 2003; Attal & Lavé, 2006; Attal et al., 2015). We find that landlide D_{84} values rarely exceed 100 mm, probably because landslides are generally shallow, mobilising the top few decimeters to meters of bedrock, which tend to be significantly weathered and fractured.

We suggest that the correlation between the coarse fraction of fluvial export and fluvial incision (Fig. 10a and b), is best explained by a combination of enhanced coarse landslide supply and transport capacity on incised catchments, given that more deeply incised catchments tend to have greater long-term rates of landsliding (e.g. Larsen and Montgomery, 2012). This coarsening cannot be explained well by only invoking differences in the discharge (drainage area) of these catchments (Fig. 10c and d), so the original grain size supplied to these rivers must play an important role, as found in other areas (Attal et al., 2015). Figure 11 also demonstrates the importance of hillslope grain size supply in determining the grain size distributions of fluvial sediment, with the relative enrichment in coarser particles in the fluvial export probably reflecting both the successive hillslope inputs downstream and the preferential transport of finer particles away from the catchment outlets. Our larger data set expands on previous findings that show that hillslope supply dominates fluvial grain size distributions in central and southern Italy (Ibbeken, 1983; Le Pera & Sorriso-Valvo, 2000; Whittaker et al., 2010). These results (Fig. 11) support findings from Allen et al. (2016), who observed that the

This article is protected by copyright. All rights reserved.

statistical properties of the grain size distributions supplied from hillslopes and proximal fluvial sediments in southern Italy are similar. However, Allen et al. (2016) also noted that fluvial sediment experiences some homogenization, which probably explains why the influence of hillslope supply is harder to differentiate from the transport control in D_{50} values (Fig. 10b and d).

Overall, this study refines predictions of grain size supply from hillslopes (e.g. Allen et al., 2015; Sklar et al., 2015), and indicate that lithology should be considered by numerical models more broadly than simply its effect on bedrock erodibility (c.f. Whipple & Tucker, 2002; Roy et al., 2015). Our data demonstrates that grain size supply can vary depending on lithology and delivery process, but in a potentially predictable way. Therefore, the observed coupling between grain size supply and bedrock erodibility (expressed both through more intense weathering or landsliding), could be readily incorporated into models of basin stratigraphy (e.g. Armitage et al., 2011; Allen et al., 2015, 2016), coupled models of landscape response and sediment flux (e.g. Cowie et al., 2006; Allen et al., 2013), or sediment flux-dependent models of fluvial incision (e.g. Sklar & Dietrich, 2006; Cowie et al., 2008).

CONCLUSIONS

We examined the lithological controls on hillslope sediment supply along normal faults in southern Italy, by combining data from a newly compiled landslide inventory and field surveys on rock strength and grains size supply. Our data reveal a dual control of rock strength and lithology on hillslope sediment fluxes, by modulating landslide activity and the grain size distributions delivered by weathering outcrops and landslides. We find that rock strength influences the abundance of steep slopes and landslides, and landslide area-frequency distributions, particularly for smaller landslide sizes, but it exerts a minor control on the frequency decay of larger landslides and on landslide area-volume scaling. Overall, landsliding in southern Italy is dominated by small and medium, shallow landslides (85% of them <0.1 km^2 and excavating <3 m deep, with β=2.3), which generate large landslide densities in the catchments (3-70%), and probably have a considerable impact on sediment fluxes. Rock strength, which captures the degree of weathering and fracturing, also controls the grain size supply from bedrock outcrops, which generally coarsens by ~10 mm for each 10-point increment in Schmidt hammer rebound values. Furthermore, lithology seems to

This article is protected by copyright. All rights reserved.

Accepted Article

influence the degree of coarsening of landslide supply with respect to weathering, perhaps through indirectly controlling the style of landsliding. Finally, we show that more incised catchments supply significantly coarser grain size distributions, due to the combination of enhanced landsliding and transport capacity.

ACKOWLEDGEMENTS

DRB and MD were funded by an Imperial College Janet Watson Bursary, awarded by the Department of Earth Science and Engineering of Imperial College London. Field campaigns were generously supported by research grants to DRB from the Geological Society of London, the British Society for Geomorphology (BSG) and the British Sedimentological Research Group (BSRG). The authors would like to thank Leonard Sklar, one anonymous reviewer, and the ESPL associate editor, for their very constructive comments that helped improve the manuscript.

Accepted Article

This article is protected by copyright. All rights reserved.

REFERENCES

Allen, P.A., Armitage, J.J., Whittaker, A.C., Michael, N.A., Roda-Boluda, D., D'Arcy, M., 2015. Fragmentation model of the grain-size mix of sediment supplied to basins. Journal of Geology 123, 405-427.

Allen, P.A., Michael, N.A., D'Arcy, M., Roda-Boluda, D.C., Whittaker, A.C., Duller, R.A., Armitage, J.J., 2016. Fractionation of grain size in terrestrial sediment routing systems. Basin Research 29 (2), 180-202

Amato, A., Aucelli, P., Cinque, A., 2003. The long-term denudation rate in the Southern Apennines Chain (Italy): a GIS-aided estimation of the rock volumes eroded since middle Pleistocene time. Quaternary International 101, 3-11.

Amato, A., Montone, P., 1997. Present-day stress field and active tectonics in southern peninsular Italy. Geophysical Journal International 130, 519-534.

Antronico, L., Greco, R., Robustelli, G., Sorriso-Valvo, M., 2015. Short-term evolution of an active basin–fan system, Aspromonte, south Italy. Geomorphology 228, 536-551.

Armitage, J.J., Duller, R.A., Whittaker, A.C., Allen, P.A., 2011. Transformation of tectonic and climatic signals from source to sedimentary archive. Nature Geoscience 4, 231-235.

Attal, M., Lavé, J., 2006. Changes of bedload characteristics along the Marsyandi River (central Nepal): Implications for understanding hillslope sediment supply, sediment load evolution along fluvial networks, and denudation in active orogenic belts. Tectonics, climate, and landscape evolution 398, 143.

Attal, M., Lavé, J., 2009. Pebble abrasion during fluvial transport: Experimental results and implications for the evolution of the sediment load along rivers. Journal of Geophysical Research: Earth Surface 114.

Attal, M., Mudd, S., Hurst, M., Weinman, B., Yoo, K., Naylor, M., 2015. Impact of change in erosion rate and landscape steepness on hillslope and fluvial sediments grain size in the Feather River Basin (Sierra Nevada, California). Earth Surface Dynamics Discussions 2, 1047-1092.

Aydin, A., Basu, A., 2005. The Schmidt hammer in rock material characterization. Engineering Geology 81, 1-14.

This article is protected by copyright. All rights reserved.

Barchi, M., Amato, A., Cippitelli, G., ENI, D.A., San Donato Milanese, M., Merlini, S., Montone, P., 2006. Extensional tectonics and seismicity in the axial zone of the Southern Apennines. Boll. Soc. Geol. It.(Italian Journal of Geosciences).

Bianchini, S., Cigna, F., Righini, G., Proietti, C., Casagli, N., 2012. Landslide hotspot mapping by means of persistent scatterer interferometry. Environmental Earth Sciences 67, 1155-1172.

Binnie, S.A., Phillips, W.M., Summerfield, M.A., Fifield, L.K., 2007. Tectonic uplift, threshold hillslopes, and denudation rates in a developing mountain range. Geology 35, 743-746.

Borgomeo, E., Hebditch, K.V., Whittaker, A.C., Lonergan, L., 2014. Characterising the spatial distribution, frequency and geomorphic controls on landslide occurrence, Molise, Italy. Geomorphology 226, 148-161.

Borrelli, L., Perri, F., Critelli, S., Gullà, G., 2014. Characterization of granitoid and gneissic weathering profiles of the Mucone River basin (Calabria, southern Italy). Catena 113, 325-340.

Burbank, D.W., Leland, J., Fielding, E., Anderson, R.S., Brozovic, N., Reid, M.R., Duncan, C., 1996. Bedrock incision, rock uplift and threshold hillslopes in the northwestern Himalayas. Nature 379, 505-510.

Calcaterra, D., Parise, M., 2005. Landslide types and their relationships with weathering in a Calabrian basin, southern Italy. Bulletin of Engineering Geology and the Environment 64, 193-207.

Calcaterra, D., Parise, M., 2010. Weathering in the crystalline rocks of Calabria, Italy, and relationships to landslides. Geological Society, London, Engineering Geology Special Publications 23, 105-130.

Casagli, N., Ermini, L., ROSati, G., 2003. Determining grain size distribution of the material composing landslide dams in the Northern Apennines: sampling and processing methods. Engineering Geology 69, 83-97.

Catalano, S., De Guidi, G., Monaco, C., Tortorici, G., Tortorici, L., 2008. Active faulting and seismicity along the Siculo–Calabrian Rift Zone (southern Italy). Tectonophysics 453, 177-192.

Cinque, A., Ascione, A., Caiazzo, C., 2000. Distribuzione spazio-temporale e caratterizzazione della fagliazione quaternaria in Appennino meridionale. Le Ricerche del GNDT nel Campo Della Pericolosità Sismica (1996 e1999). CNR-GNDT, Rome, pp. 203e218 (in Italian).

This article is protected by copyright. All rights reserved.

Accepted Article

Clarke, B.A., Burbank, D.W., 2010. Bedrock fracturing, threshold hillslopes, and limits to the magnitude of bedrock landslides. Earth and Planetary Science Letters 297, 577-586.

Coico, P., Calcaterra, D., De Pippo, T., Guida, D., 2013. A preliminary perspective on landslide dams of Campania region, Italy, Landslide Science and Practice. Springer, pp. 83-90.

Colella, A., Lapenna, V., Rizzo, E., 2004. High-resolution imaging of the High Agri Valley basin (southern Italy) with electrical resistivity tomography. Tectonophysics 386, 29-40.

Conforti, M., Aucelli, P.P., Robustelli, G., Scarciglia, F., 2011. Geomorphology and GIS analysis for mapping gully erosion susceptibility in the Turbolo stream catchment (Northern Calabria, Italy). Natural hazards 56, 881-898.

Conforti, M., Muto, F., Rago, V., Critelli, S., 2014. Landslide inventory map of north-eastern Calabria (South Italy). Journal of Maps 10, 90-102.

Cowie, P.A., Whittaker, A.C., Attal, M., Roberts, G., Tucker, G.E., Ganas, A., 2008. New constraints on sediment-flux–dependent river incision: Implications for extracting tectonic signals from river profiles. Geology 36, 535-538.

Cyr, A.J., Granger, D.E., Olivetti, V., Molin, P., 2010. Quantifying rock uplift rates using channel steepness and cosmogenic nuclide–determined erosion rates: Examples from northern and southern Italy. Lithosphere 2, 188-198.

D'Arcy, M., Whittaker, A.C., Roda Boluda, D.C., 2016. Measuring alluvial fan sensitivity to past climate changes using a self-similarity approach to grain size fining, Death Valley, California. Sedimentology.

Densmore, A.L., Anderson, R.S., McAdoo, B.G., Ellis, M.A., 1997. Hillslope evolution by bedrock landslides. Science 275, 369-372.

Densmore, A.L., Ellis, M.A., Anderson, R.S., 1998. Landsliding and the evolution of normal fault-bounded mountains. Journal of geophysical research: solid earth. 103, 15203-15219.

Dunning, S., 2006. The grain size distribution of rock-avalanche deposits in valley-confined settings. Ital J Eng Geol Environ 1, 117-121.

Egholm, D.L., Knudsen, M.F., Sandiford, M., 2013. Lifespan of mountain ranges scaled by feedbacks between landsliding and erosion by rivers. Nature 498, 475-478.

This article is protected by copyright. All rights reserved.

Accepted Article

Faccenna, C., Molin, P., Orecchio, B., Olivetti, V., Bellier, O., Funiciello, F., Minelli, L., Piromallo, C. & Billi, A. 2011. Topography of the Calabria subduction zone (southern Italy): clues for the origin of Mt. Etna. *Tectonics*, **30**.

Falconi, L., Campolo, D., Leoni, G., Lumaca, S. & Puglisi, C. 2013. Geomorphology hazard assessment of Giampilieri and Briga river basins after the rainfall event on the October 1, 2009 (Sicily, Italy). *Landslide Science and Practice. Springer, 533-540.*

Fazio, E., Cirrincione, R., Pezzino, A., 2015. Tectono-metamorphic map of the south-western flank of the Aspromonte Massif (southern Calabria-Italy). Journal of Maps 11, 85-100.

Ferro, V., Porto, P., 2012. Identifying a dominant discharge for natural rivers in southern Italy. Geomorphology 139, 313-321.`

Frattini, P. & Crosta, G.B. 2013. The role of material properties and landscape morphology on landslide size distributions. *Earth and Planetary Science Letters*, **361**, 310-319.

Gallen, S. F., Clark, M. K., & Godt, J. W. (2015). Coseismic landslides reveal near-surface rock strength in a high-relief, tectonically active setting. *Geology, 43*(1), 11-14. doi: 10.1130/g36080.1

Galli, M., Ardizzone, F., Cardinali, M., Guzzetti, F., Reichenbach, P., 2008. Comparing landslide inventory maps. Geomorphology 94, 268-289.

Galli, P., Bosi, V., 2002. Paleoseismology along the Cittanova fault: Implications for seismotectonics and earthquake recurrence in Calabria (southern Italy). Journal of Geophysical Research: Solid Earth (1978–2012) 107, ETG 1-1-ETG 1-19.

Galli, P.A., Peronace, E., 2015. Low slip rates and multimillennial return times for Mw 7 earthquake faults in southern Calabria (Italy). Geophysical Research Letters 42, 5258-5265.

Giocoli, A., Stabile, T., Adurno, I., Perrone, A., Gallipoli, M., Gueguen, E., Norelli, E., Piscitelli, S., 2015. Geological and geophysical characterization of the south-eastern side of the High Agri Valley (southern Apennines, Italy). Natural Hazards and Earth System Science 15, 315-323.

Gioia, D., Martino, C., Schiattarella, M., 2011. Long-to short-term denudation rates in the southern Apennines: geomorphological markers and chronological constraints. Geologica Carpathica 62, 27-41.

This article is protected by copyright. All rights reserved.

Goswami, R., Mitchell, N.C., Brocklehurst, S.H., 2011. Distribution and causes of landslides in the eastern Peloritani of NE Sicily and western Aspromonte of SW Calabria, Italy. Geomorphology 132, 111-122.

Goswami, R., Mitchell, N.C., Brocklehurst, S.H., Argnani, A., 2016. Linking subaerial erosion with submarine geomorphology in the western Ionian Sea (south of the Messina Strait), Italy. Basin Research.

Goudie, A.S., 2006. The Schmidt hammer in geomorphological research. Progress in Physical Geography 30, 703-718.

Guadagno, F.M., Revellino, P., 2005. Debris avalanches and debris flows of the Campania Region (southern Italy), Debris-flow hazards and related phenomena. Springer, pp. 489-518.

Gullà, G., Antronico, L., Iaquinta, P., Terranova, O., 2008. Susceptibility and triggering scenarios at a regional scale for shallow landslides. Geomorphology 99, 39-58.

Guzzetti, F., Ardizzone, F., Cardinali, M., Rossi, M., Valigi, D., 2009. Landslide volumes and landslide mobilization rates in Umbria, central Italy. Earth and Planetary Science Letters 279, 222-229.

Guzzetti, F., Malamud, B.D., Turcotte, D.L., Reichenbach, P., 2002. Power-law correlations of landslide areas in central Italy. Earth and Planetary Science Letters 195, 169-183.

Guzzetti, F., Mondini, A.C., Cardinali, M., Fiorucci, F., Santangelo, M., Chang, K.-T., 2012. Landslide inventory maps: New tools for an old problem. Earth-Science Reviews 112, 42-66.

Hewitt, K., 1999. Quaternary moraines vs catastrophic rock avalanches in the Karakoram Himalaya, northern Pakistan. Quaternary research 51, 220-237.

Hovius, N., Stark, C.P., Allen, P.A., 1997. Sediment flux from a mountain belt derived by landslide mapping. Geology 25, 231-234.

.Huang, J.-C., Lee, T.-Y., Teng, T.-Y., Chen, Y.-C., Huang, C.-Y. & Lee, C.-T. 2014. Validating the operational bias and hypothesis of universal exponent in landslide frequency-area distribution. *PloS one*, **9**, e98125.

Ibbeken, H., 1983. Jointed source rock and fluvial gravels controlled by Rosin's law: a grain-size study in Calabria, South Italy. Journal of Sedimentary Research 53.

This article is protected by copyright. All rights reserved.

Accepted Article

Ibbeken, H., Schleyer, R., 1991. Source and sediment: a case study of provenance and mass balance at an active plate margin (Calabria, Southern Italy). Springer Science & Business Media.

Ietto, F., Donato, F.F., Ietto, A., 2007. Recent reverse faults and landslides in granitoid weathered profiles, Serre Mountains (southern Calabria, Italy). Geomorphology 87, 196-206.

Jerolmack, D.J. & Paola, C. 2010. Shredding of environmental signals by sediment transport. *Geophysical Research Letters*, **37**.

Korup, O., 2008. Rock type leaves topographic signature in landslide-dominated mountain ranges. Geophysical Research Letters 35, L11402.

Korup, O., Görüm, T., Hayakawa, Y., 2012. Without power? Landslide inventories in the face of climate change. Earth Surface Processes and Landforms 37, 92-99.

Korup, O., Schlunegger, F., 2009. Rock-type control on erosion-induced uplift, eastern Swiss Alps. Earth and Planetary Science Letters 278, 278-285.

Krumbein, W.C., Tisdel, F.W., 1940. Size distribution of source rocks of sediments. American Journal of Science 238, 296-305.

Larsen, I.J., Montgomery, D.R., 2012. Landslide erosion coupled to tectonics and river incision. Nature Geoscience 5, 468-473.

Larsen, I.J., Montgomery, D.R., Korup, O., 2010. Landslide erosion controlled by hillslope material. Nature Geoscience 3, 247-251.

Lazzari, M., Schiattarella, M., 2010. Estimating long to short-term erosion rates of fluvial vs mass movement processes: an example from the axial zone of the southern Italian Apennines. Italian Journal of Agronomy 5, 57-66.

Le Pera, E., Sorriso-Valvo, M., 2000. Weathering, erosion and sediment composition in a high-gradient river, Calabria, Italy. Earth Surface Processes and Landforms 25, 277-292.

Malamud, B.D., Turcotte, D.L., Guzzetti, F., Reichenbach, P., 2004. Landslide inventories and their statistical properties. Earth Surface Processes and Landforms 29, 687-711.

Malamud, B.D., Turcotte, D.L., Guzzetti, F., Reichenbach, P., 2004b. Landslides, earthquakes, and erosion. Earth and Planetary Science Letters 229, 45-59.

This article is protected by copyright. All rights reserved.

Marshall, J.A. & Sklar, L.S. 2012. Mining soil databases for landscape-scale patterns in the abundance and size distribution of hillslope rock fragments. *Earth Surface Processes and Landforms*, **37**, 287-300.

Michael, N.A., Whittaker, A.C., Carter, A. & Allen, P.A. 2014. Volumetric budget and grain-size fractionation of a geological sediment routing system: Eocene Escanilla Formation, south-central Pyrenees. *Geological Society of America Bulletin*, **126**, 585-599.

Minaeian, B., Ahangari, K., 2013. Estimation of uniaxial compressive strength based on P-wave and Schmidt hammer rebound using statistical method. Arabian Journal of Geosciences 6, 1925-1931.

Miyauchi, T., Dai Pra, G., Sylos Labini, S., 1994. Geochronology of Pleistocene marine terraces and regional tectonics in the Tyrrhenian coast of South Calabria, Italy. Il Quaternario 7, 17-34.

Monaco, C., Tortorici, L., 2000. Active faulting in the Calabrian arc and eastern Sicily. Journal of Geodynamics 29, 407-424.

Montgomery, D.R., Brandon, M.T., 2002. Topographic controls on erosion rates in tectonically active mountain ranges. Earth and Planetary Science Letters 201, 481-489.

Moore, J.R., Sanders, J.W., Dietrich, W.E., Glaser, S.D., 2009. Influence of rock mass strength on the erosion rate of alpine cliffs. Earth Surface Processes and Landforms 34, 1339-1352.

Mueller, E.R., Smith, M.E., Pitlick, J., 2016. Lithology-controlled evolution of stream bed sediment and basin-scale sediment yields in adjacent mountain watersheds, Idaho, USA. Earth Surface Processes and Landforms.

O'Connor, J.E., Mangano, J.F., Anderson, S.W., Wallick, J.R., Jones, K.L., Keith, M.K., 2014. Geologic and physiographic controls on bed-material yield, transport, and channel morphology for alluvial and bedrock rivers, western Oregon. Geological Society of America Bulletin, B30831. 30831.

Olivetti, V., Cyr, A.J., Molin, P., Faccenna, C., Granger, D.E., 2012. Uplift history of the Sila Massif, southern Italy, deciphered from cosmogenic 10Be erosion rates and river longitudinal profile analysis. Tectonics 31.

Ouimet, W.B., Whipple, K.X., Granger, D.E., 2009. Beyond threshold hillslopes: Channel adjustment to base-level fall in tectonically active mountain ranges. Geology 37, 579-582.

This article is protected by copyright. All rights reserved.

Pantosti, D., Valensise, G., 1990. Faulting mechanism and complexity of the November 23, 1980, Campania-Lucania earthquake, inferred from surface observations. Journal of Geophysical Research: Solid Earth (1978–2012) 95, 15319-15341.

Papanikolaou, I.D., Roberts, G.P., 2007. Geometry, kinematics and deformation rates along the active normal fault system in the southern Apennines: Implications for fault growth. Journal of Structural Geology 29, 166-188.

Patacca, E., Scandone, P., 2007. Constraints on the interpretation of the CROP-04 seismic line derived from Plio–Pleistocene foredeep and thrust-sheet-top deposits (southern Apennines, Italy). CROP-04. Edited by A. Mazzotti, E. Patacca, and P. Scandone. Bollettino della Società Geologica Italiana, Special, 241-256.

Petrucci, O., Pasqua, A., 2009. A methodological approach to characterise Landslide Periods based on historical series of rainfall and landslide damage. Natural Hazards and Earth System Sciences 9, 1655-1670.

Petrucci, O., Polemio, M., 2000. Catastrophic Geomophological Events and the role of rainfalls in South-Eastern Calabria (Southern Italy), Mediterranean Storms Plinius Conference'99. Editoriale Bios.

Petrucci, O., Polemio, M., 2009. The role of meteorological and climatic conditions in the occurrence of damaging hydro-geologic events in Southern Italy. Natural Hazards and Earth System Sciences 9, 105-118.

Petrucci, O., Polemio, M., Pasqua, A., 2009. Analysis of damaging hydrogeological events: the case of the Calabria Region (Southern Italy). Environmental Management 43, 483-495.

Polemio, M., Lonigro, T., 2013. Climate Variability and Landslide Occurrence in Apulia (Southern Italy), Landslide Science and Practice. Springer, pp. 37-41.

Polemio, M., Lonigro, T., 2015. Trends in climate, short-duration rainfall, and damaging hydrogeological events (Apulia, Southern Italy). Natural hazards 75, 515-540.

Portenga, E.W., Bierman, P.R., 2011. Understanding Earth's eroding surface with 10 Be. GSA Today 21, 4-10.

Riebe, C.S., Sklar, L.S., Lukens, C.E., Shuster, D.L., 2015. Climate and topography control the size and flux of sediment produced on steep mountain slopes. Proceedings of the National Academy of Sciences 112, 15574-15579.

This article is protected by copyright. All rights reserved.

Accepted Article

Roda-Boluda, D.C., Whittaker, A.C., 2016. Normal fault evolution and coupled landscape response: examples from the Southern Apennines, Italy. Basin Research.

Roda-Boluda, D.C. & Whittaker, A.C. 2017. Structural and geomorphological constraints on active normal faulting and landscape evolution in Calabria, Italy. Journal of the Geological Society.

Roda-Boluda, D., D'Arcy, M., Whittaker, A., Gheorghiu, D., & Rodes, A. 2017. ^{10}Be erosion rates controlled by normal fault activity through incision and landslide occurrence. Paper presented at the EGU General Assembly Conference Abstracts, 19, 4899.

Roda-Boluda, D. 2017. Characterising landscape response, erosional supply and sediment flux along active normal faults. PhD thesis. Imperial College London.

Santangelo, M., Gioia, D., Cardinali, M., Guzzetti, F., Schiattarella, M., 2013. Interplay between mass movement and fluvial network organization: An example from southern Apennines, Italy. Geomorphology 188, 54-67.

Scarciglia, F., Critelli, S., Borrelli, L., Coniglio, S., Muto, F., Perri, F., 2016. Weathering profiles in granitoid rocks of the Sila Massif uplands, Calabria, southern Italy: New insights into their formation processes and rates. Sedimentary Geology 336, 46-67.

Schmidt, K.M., Montgomery, D.R., 1995. Limits to relief. Science 270, 617.

Selby, M., 1980. A rock mass strength classification for geomorphic purposes: with tests from Antarctica and New Zealand. Zeitschrift für Geomorphologie 24, 31-51.

Selby, M., 1982. Controls on the stability and inclinations of hillslopes formed on hard rock. Earth Surface Processes and Landforms 7, 449-467.

Simoni, A., Ponza, A., Picotti, V., Berti, M., 2013. Landslide-Related Sediment Yield Rate in a Large Apenninic Catchment, Landslide Science and Practice. Springer, pp. 307-313.

Simpson, G. & Castelltort, S. 2012. Model shows that rivers transmit high-frequency climate cycles to the sedimentary record. *Geology*, **40**, 1131-1134.

Sklar, L.S., Dietrich, W.E., 2001. Sediment and rock strength controls on river incision into bedrock. Geology 29, 1087-1090.

Sklar, L.S. & Dietrich, W.E. 2004. A mechanistic model for river incision into bedrock by saltating bed load. *Water resources research*, **40**, W06301.Sklar, L.S., Dietrich, W.E., 2006. The role of sediment in controlling steady-state bedrock channel slope: Implications of the saltation–abrasion incision model. Geomorphology 82, 58-83.

This article is protected by copyright. All rights reserved.

Sklar, L.S., Dietrich, W.E., Foufoula-Georgiou, E., Lashermes, B. & Bellugi, D. 2006b. Do gravel bed river size distributions record channel network structure. *Water resources research*, **42**, W06D18.

Sklar, L.S., Riebe, C.S., Marshall, J.A., Genetti, J., Leclere, S., Lukens, C.L., Merces, V., 2016. The problem of predicting the size distribution of sediment supplied by hillslopes to rivers. Geomorphology.

Stark, C.P., Hovius, N., 2001. The characterization of landslide size distributions. Geophysical Research Letters 28, 1091-1094.

Summa, V., Margiotta, S., Colaiacovo, R., Giannossi, M., 2015. The influence of the grain-size, mineralogical and geochemical composition on the Verdesca landslide. Natural Hazards and Earth System Sciences 15, 135-146.

Terranova, O., Antronico, L., Coscarelli, R., Iaquinta, P., 2009. Soil erosion risk scenarios in the Mediterranean environment using RUSLE and GIS: an application model for Calabria (southern Italy). Geomorphology 112, 228-245.

Terranova, O., Antronico, L., Gullà, G., 2007. Landslide triggering scenarios in homogeneous geological contexts: The area surrounding Acri (Calabria, Italy). Geomorphology 87, 250-267.

Trigila, A., Iadanza, C., Spizzichino, D., 2010. Quality assessment of the Italian Landslide Inventory using GIS processing. Landslides 7, 455-470.

Turowski, J. M., Rickenmann, D., & Dadson, S. J. (2010). The partitioning of the total sediment load of a river into suspended load and bedload: a review of empirical data. *Sedimentology, 57*(4), 1126-1146.

Van Den Eeckhaut, M., Poesen, J., Govers, G., Verstraeten, G., Demoulin, A., 2007. Characteristics of the size distribution of recent and historical landslides in a populated hilly region. Earth and Planetary Science Letters 256, 588-603.

Villani, F., Pierdominici, S., 2010. Late Quaternary tectonics of the Vallo di Diano basin (southern Apennines, Italy). Quaternary Science Reviews 29, 3167-3183.

Vivenzio, J., 1783. Istoria e teoria de'tremuoti in generale ed in particolare di quelli della Calabria, e di Messina del 1783.-Napoli, Stamperia regale 1783. Stamperia regale.

von Eynatten, H., Tolosana-Delgado, R., Karius, V., Bachmann, K., Caracciolo, L., 2016. Sediment generation in humid Mediterranean setting: Grain-size and source-

This article is protected by copyright. All rights reserved.

rock control on sediment geochemistry and mineralogy (Sila Massif, Calabria). Sedimentary Geology 336, 68-80.

Whipple, K.X., Tucker, G.E., 2002. Implications of sediment-flux-dependent river incision models for landscape evolution. Journal of Geophysical Research 107, 2039.

White, E.P., Enquist, B.J. & Green, J.L. 2008. On estimating the exponent of power-law frequency distributions. *Ecology*, **89**, 905-912.

Whittaker, A.C., Attal, M., Allen, P.A., 2010. Characterising the origin, nature and fate of sediment exported from catchments perturbed by active tectonics. Basin Research 22, 809-828.

Whittaker, A.C., Duller, R.A., Springett, J., Smithells, R.A., Whitchurch, A.L., Allen, P.A., 2011. Decoding downstream trends in stratigraphic grain size as a function of tectonic subsidence and sediment supply. Geological Society of America Bulletin 123, 1363-1382.

Wolcott, J., 1988. Nonfluvial control of bimodal grain-size distributions in river-bed gravels. Journal of Sedimentary Research 58.

Wolman, M.G., 1954. A method of sampling coarse river-bed material. Eos, Transactions American Geophysical Union 35, 951-956.

York, D. (1968). Least squares fitting of a straight line with correlated errors. *Earth and Planetary Science Letters, 5*, 320-324.

Zhao, T., Crosta, G. B., Utili, S., & De Blasio, F. V. (2017). Investigation of rock fragmentation during rockfalls and rock avalanches via 3-D discrete element analyses. *Journal of Geophysical Research: Earth Surface, 122*(3), 678-695.

Accepted Article

This article is protected by copyright. All rights reserved.

Accepted Article

Table 1. Bedrock outcrops Schmidth hammer rebound measurements and weathering products grain size data.

Lithology	Bedrock field locality[†Bedrock field locality]	Latitude (N)	Longitude (E)	Schmidt hammer rebound, mean value	Schmidt hammer rebound, standard error	Mean Schmidt hammer rebound value ± standard error	D_{50} (mm)	D_{84} (mm)
Sandstones	1	40°21'35.2"	15°56'58.4"	24.9	2.3	17.4 ± 2.3	7	50
	2	40°22'35.9"	15°55'14.0"	26.5	1.6		15	50
	3	40°15'06.2"	15°59'52.6"	15.4	1.6		17	48
	4	40°14'20.5"	15°57'11.9"	11.7	1.7		18	46
	5	40°31'03.8"	15°33'23.8"	22.7	1.8		25	45
	6	40°25'15.5"	15°40'08.2"	16.1	2.4		24	46
	7	40°31'16.2"	15°36'36.5"	10.0	0.0		21	45
	8	40°20'41.2"	15°53'21.1"	12.2	0.6		14	28
Carbonates	9	40°31'05.3"	15°33'16.1"	32.4	1.0	30.0 ± 3.0	24	59
	10	40°22'25.2"	15°49'37.3"	10.0	0.0		19	41
	11	40°24'53.3"	15°44'00.2"	17.5	2.8		19	37
	12	40°27'36.3"	15°33'27.3"	44.0	1.3		26	66
	13	40°23'49.2"	15°43'40.7"	19.1	3.4		22	42
	14	40°30'44.9"	15°32'38.2"	44.8	1.6		30	80
	15	40°23'32.2"	15°37'59.0"	28.2	2.6		21	65
	16	40°21'50.7"	15°48'48.5"	21.1	3.1		23	48
	17	40°16'12.5"	15°44'45.8"	37.4	2.5		14	45
	18	40°16'19.5"	15°44'32.7"	37.0	1.7		20	50
	19	40°25'30.8"	15°45'53.1"	38.6	2.5		26	65
	20	40°25'24.0"	15°46'22.9"	42.5	2.3		28	72
	21	40°27'59.2"	15°44'27.7"	28.5	1.6		22	54
	22	40°27'59.3"	15°44'27.1"	19.2	3.4		18	36
Red Chert	23	40°21'14.0"	15°40'05.2"	10.0	0.0	14.1 ± 4.1	22	51
	24	40°23'59.7"	15°49'57.6"	18.1	2.7		23	45
Gneisses and Schists	25	38°13'39.8"	15°54'23.4"	38.6	1.8	26.0 ± 5.0 / 24.9 ± 3.0*	25	58
	26	38°12'42.0"	15°54'57.5"	37.8	1.6		35	71
	27	38°03'42.4"	15°47'15.7"	33.3	2.2		29	51
	28	39°33'24.1"	16°19'44.1"	21.0	8.2		23	71
	29	39°33'37.3"	16°19'39.6"	15.4	2.2		29	66
	30	39°26'09.1"	16°07'09.2"	10.0	0.0		-	-
Granites	31	39°24'59.0"	16°22'42.9"	10.0	0.0	21.1 ± 7.4 / 21.3 ± 4.5*	5	16
	32	39°23'37.1"	16°32'46.3"	18.1	1.6		21	42
	33	39°28'24.6"	16°24'11.7"	35.1	1.7		32	60
Pleistocene deposits	34	39°20'27.4"	16°08'49.0"	10.0	0.0	15.2 ± 5.2	-	-
	35	39°27'40.7"	16°07'10.7"	20.4	1.3		-	-

†A version of Fig. 1 with labelled field localities can be found in the supplementary material.

* denotes that these mean values and standard errors have been calculated incorporating the Schmidt hammer rebound values estimated from Borrelli et al. (2014) data (11 localities on the granites and 24 on the gneiss and schists; see supplementary material).

This article is protected by copyright. All rights reserved.

Table 2. Field data for calibration of landslide area-volume scaling relationship.

Field locality†	Latitude (N)	Longitude (E)	Lithology	Field estimate % of fine material < 1 mm *	Length (m)	Width (m)	Height (m)	Radius (m)	Best fit geometric shape	Area estimate (m^2)	Volume estimate (m^3)
D40	40°15'05.9''	15°59'55.7''	Sandstone	50%	810	501	9	-	cuboid	405000	3645000
D76	38°02'52.2''	15°45'36.6''	Gneiss	40%	-	-	12	27	half-cone	2290	4580
D81	38°07'03.5''	15°50'37.4''	Gneiss	20%	-	-	8	7	half-cone	154	205
D112	39°28'52.8''	16°18'16.4''	Gneiss	15%	-	-	7	15	half-cone	707	825
J3	39°28'24.6''	16°24'11.7''	Granite	65%	-	-	11	18	half-cone	1018	1866
J22	39°29'36.4''	16°06'24.6''	Schist	15%	10	10	1.5	-	cuboid	100	150
J52	40°30'57.2''	15°35'07.0''	Carbonate	65%	-	-	4	4	half-cone	50	34
J59	40°23'01.9''	15°49'22.8''	Carbonate	70%	-	-	16	13	half-cone	531	1416
Verdesca landslide (Giocoli et al., 2015)	40°18'01.12''	15°59'29.21''	Sandstone	-	750	320	15	-	cuboid	240000	3600000

†A version of Fig. 1 with labelled field localities can be found in the supplementary material.

* i.e. proxy for bedrock-soil components of landslide type. These should be considered as minimum estimates because they are derived from the landslide surface, where some fines could have been washed away.

This article is protected by copyright. All rights reserved.

Accepted Article

Table 3. Landslides grain size data.

Lithology	Landslide field locality†Landslide field locality†Landslide field locality†	Latitude (N)	Longitude (E)	D_{50} (mm)D_{50} (mm)D_{50} (mm)	D_{84} (mm)D_{84} (mm)D_{84} (mm)
Sandstones	1	40°14'03.11"	15°56'18.6"	14	40
	2	40°15'02.9"	15°59'53.6"	31	90
	3	40°15'05.9"	15°59'55.7"	26	75
	4	40°20'56.2"	15°54'36.7"	34	62
	5	40°21'57.7"	15°55'23.1"	36	81
	6	40°22'20.7"	15°55'59.2"	25	58
	7	40°21'33.0"	15°57'19.4"	28	66
	8	40°20'40.1"	15°56'02.2"	22	50
	9*	40°20'03.6"	15°59'13.8"	44	92
	10*	40°20'08.2"	15°59'12.1"	34	62
	11*	40°20'08.2"	15°59'12.1"	18	36
	12	40°19'47.5"	15°58'28.3"	30	69
	13	40°20'17.6"	15°58'14.4"	38	93
	14*	40°14'20.7"	15°57'23.6"	32	69
	15*	40°14'20.3"	15°57'30.7"	19	42
	16	40°14'22.1"	15°57'39.6"	18	36
	17	40°26'06.1"	15°39'40.5"	25	80
Carbonates	28	40°14'22.5"	15°53'49.0"	31	56
	29	40°27'48.8"	15°44'14.9"	27	56
	30*	40°27'44.2"	15°44'15.8"	20	44
	31*	40°27'38.3"	15°44'09.5"	18	40
	32	40°27'27.1"	15°43'54.7"	32	59
	33	40°26'54.0"	15°43'49.2"	33	63
	34	40°26'51.4"	15°43'50.4"	29	61
	35	40°30'57.2"	15°35'07.0"	26	67
	36	40°22'38.3"	15°50'00.8"	30	75
	37	40°22'33.4"	15°49'54.6"	21	44
	38	40°23'00.9"	15°49'24.7"	27	48
	40	40°22'30.2"	15°49'53.5"	22	75
	41	40°27'03.8"	15°43'54.5"	21	51
Gneiss and Schists	19	38°44'07.2'	16°18'35.8"	38	87
	20	38°02'52.2"	15°45'36.6"	35	80
	21	38°07'03.5"	15°50'37.4"	39	91
	22	39°28'52.8"	16°18'16.4"	29	65
	23	39°22'26.2"	16°08'57.8"	53	100
	24*	39°25'22.3"	16°07'17.2"	25	58
	25*	39°25'23.7"	16°07'15.3"	26	69
	26	39°25'34.4"	16°07'10.4"	24	47
	27	39°29'36.4"	16°06'24.6"	48	126
Granites	18	39°28'24.4"	16°24'11.8"	52	97

†A version of Fig. 1 with labelled field localities can be found in the supplementary material.

*The asterisk indicates that grain size distributions have been measured in different localities on the same landslide deposit.

This article is protected by copyright. All rights reserved.

Table 4. Fluvial export from catchments. Catchments are listed from north to south along the faults; see supplementary information for a map with catchment identifications.

Fault	Catch-ment Id[†]	Latitude (N)	Longitude (E)	Dominant lithology (>50% of area)	Catchment area, A (km^2)	Area covered by landslides (km^2)	Catchment landslide density (%)	maximum incision depth, d_i (m)	D_{50} catchment fluvial export (mm)	D_{84} catchment fluvial export (mm)
Agri	58	40°30'33.4"	15°37'28.3"	mixed	16.4	2.7	16.3	162	16	50
Agri	59	40°28'52.8"	15°37'38.2"	sandstones	4.6	0.2	5.2	67	26	65
Agri	60	40°27'25.5"	15°39'40.4"	carbonates	27.5	2.3	8.2	242	29	74
Agri	63	40°26'15.7"	15°44'49.0"	mixed	27.0	6.6	24.4	439	42	90
Agri	67	40°22'40.2"	15°48'04.8"	mixed	11.6	0.3	2.4	390	26	80
Agri	69	40°22'22.9"	15°48'26.0"	carbonates	7.7	1.6	21.2	171	34	65
Agri	72	40°21'14.4"	15°52'40.1"	mixed	15.4	2.6	16.9	394	28	62
Agri	75	40°20'34.9"	15°55'17.0"	sandstones	32.1	5.4	17.0	408	27	83
Agri	78	40°18'58.5"	15°57'56.2"	sandstones	13.3	3.5	26.4	237	23	60
East Crati	56	39°38'09.6"	16°21'30.3"	gneiss & schists	13.5	0.6	4.6	168	28	51
East Crati	58	39°31'25.9"	16°17'22.0"	gneiss & schists	5.4	0.1	2.4	161	30	61
East Crati	59	39°29'56.7"	16°16'39.5"	sandstones	4.1	0.1	2.9	89	27	55
East Crati	97	39°28'41.0"	16°15'14.0"	granites	288.3	10.6	3.7	587	41	84
East Crati	92	39°21'05.9"	16°15'54.6"	gneiss & schists	8.0	0.5	6.3	252	28	60
East Crati	103	39°17'06.8"	16°17'40.3"	gneiss & schists	13.8	1.0	7.4	255	28	52
Cittanova	197	38°26'27.6"	16°06'15.5"	granites	13.5	0.4	2.7	219	29	59
Cittanova	205	38°25'15.1"	16°05'56.3"	mixed	21.8	6.7	30.7	353	27	65
Cittanova	211	38°22'40.9"	16°04'52.2"	granites	11.8	0.3	2.1	366	30	72
Cittanova	220	38°20'35.5"	16°03'59.0"	granites	13.5	0.7	4.9	386	31	83
Cittanova	231	38°19'10.7"	16°02"13.0"	granites	9.2	0.2	2.2	330	33	73
Cittanova	237	38°16'39.0"	15°59'41.9"	gneiss & schists	3.7	0.3	7.1	188	24	58
Cittanova	238	38°14'59.2"	18°59'05.4"	gneiss & schists	7.8	0.4	5.3	341	29	61
Cittanova	244	38°15'00.8"	15°57'21.3"	gneiss & schists	16.6	1.0	6.2	358	33	80
Armo	275	38°05'00.6"	15°43'37.6"	gneiss & schists	39.4	5.2	13.1	563	33	76
Armo	279	38°02'49.5"	15°41'48.2"	gneiss & schists	22.9	2.0	8.5	466	38	79
Armo	280	38°01'53.8"	15°39'38.4"	mixed	2.4	0.1	4.0	82	25	52

[†]A version of Fig. 1 with labelled catchments can be found in the supplementary material.

This article is protected by copyright. All rights reserved.

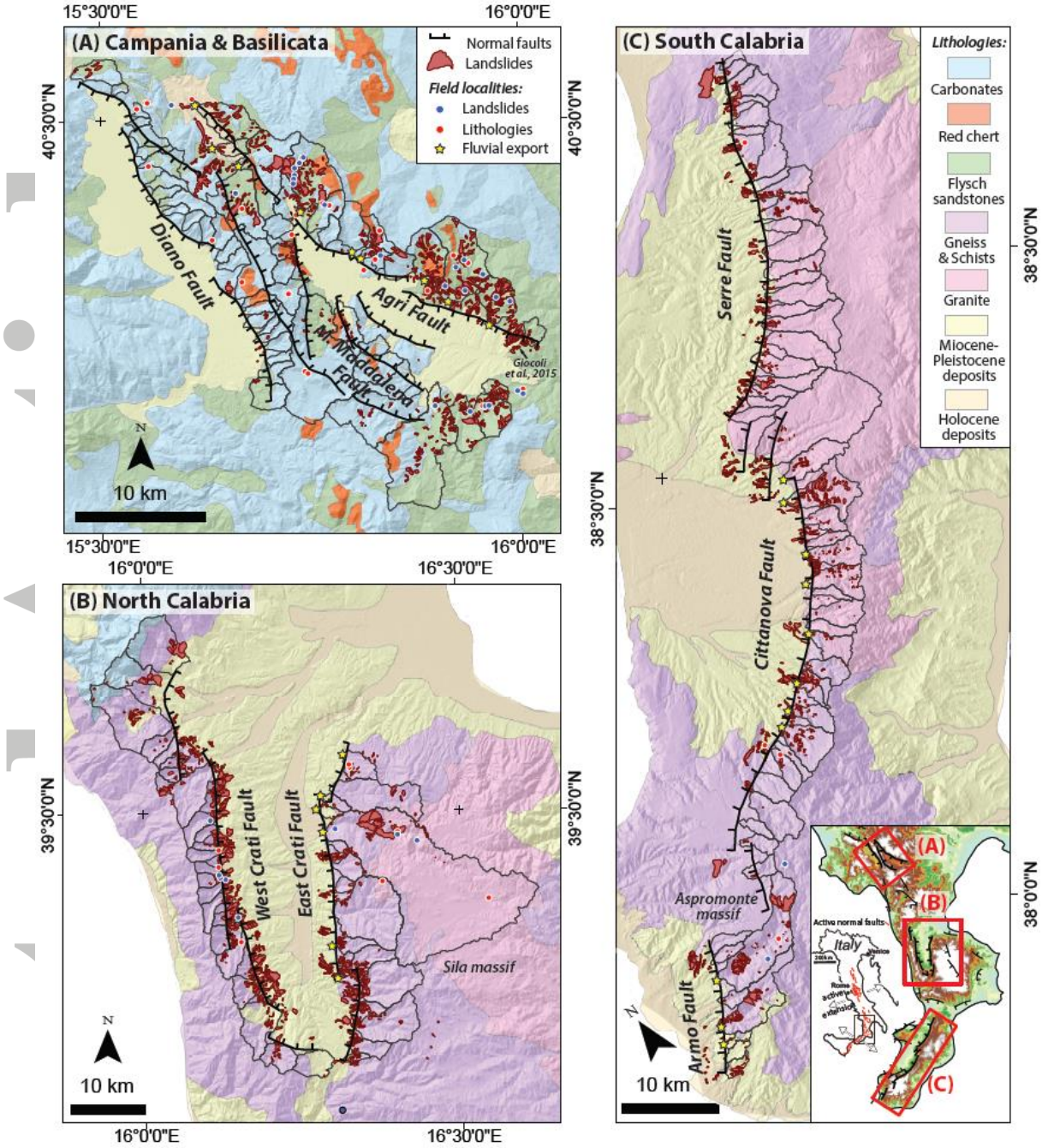


FIGURE 1

Figure 1. Simplified geologic map of the study area, showing mapped landslides, fault footwall catchments, and field sampling sites, for Campania and Basilicata (a), in the southern Apennines, northern Calabria (b) and southern Calabria (b).

This article is protected by copyright. All rights reserved.

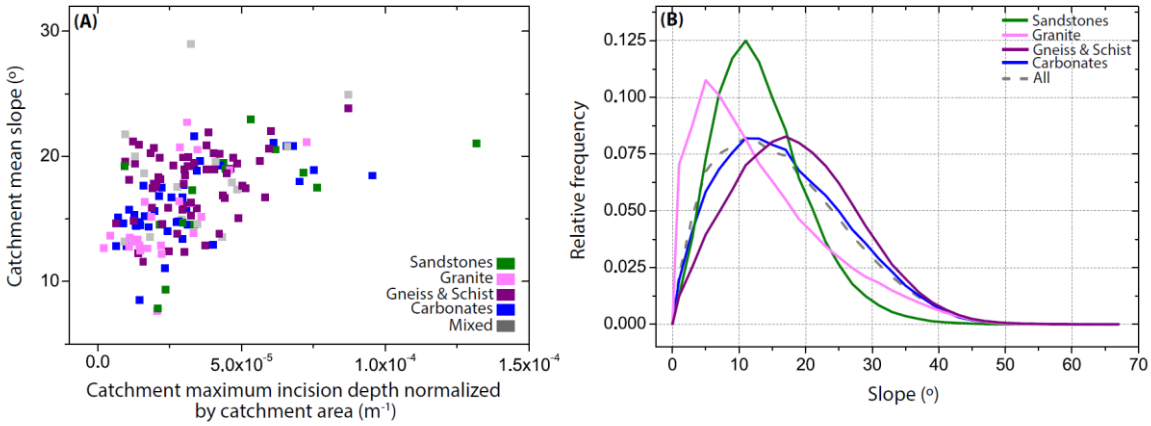


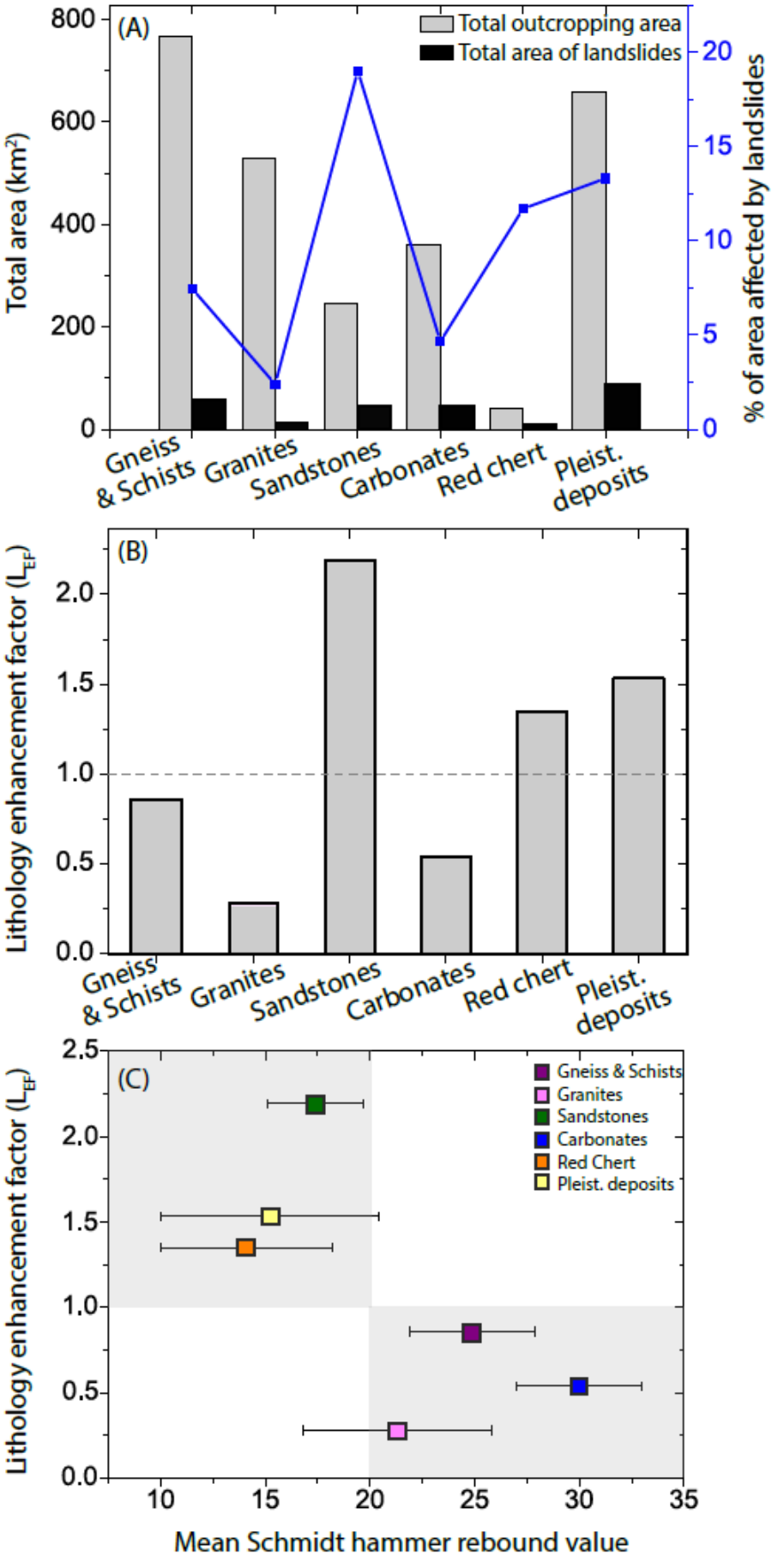
FIGURE 2

Figure 2. (a) Catchment mean slope angle against catchment maximum fluvial incision depth normalized by catchment area, for the 152 footwall catchments along the studied normal faults, colour-coded by their dominant (>50% areal coverage) lithologies. (b) Relative frequency distributions of slopes for each of the main lithologies.

Accepted Article

This article is protected by copyright. All rights reserved.

Accepted Article



This article is protected by copyright. All rights reserved.

Figure 3. (a) Total outcropping area and area covered by landslides (left axis), and proportion of area affected by landslides (right axis), for each lithological group. (b) Landslide enhancement factors (L_{EF}) for each lithologic group, calculated from Eq. 3. (c) L_{EF} values plotted against the mean Schmidt hammer rebound values, a proxy for rock strength, for each lithologic type (Table 1), including Borrelli et al.'s (2014) data for the granites and gneisses and schists (see Table S2 in the supplementary information). Error bars on the x-axis represent the standard error from the mean (Table 1).

Accepted Article

This article is protected by copyright. All rights reserved.

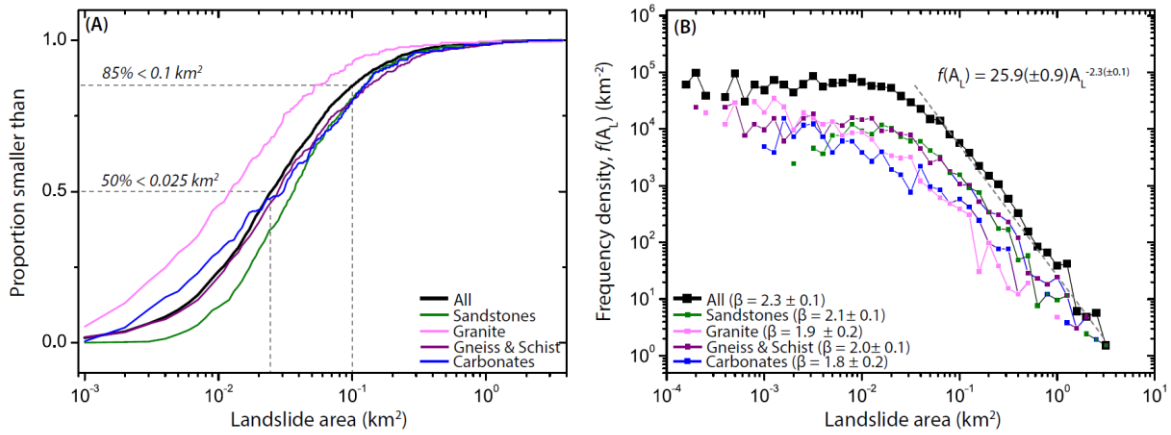


Figure 4. (a) Cumulative frequency of landslide sizes, for the overall inventory (black line) and the four main lithologies. (b) Landslide non-cumulative frequency density for increasing landslide areas, for the overall inventory (black), and the four main lithologies. The power law representing the frequency density is fitted for landslides >0.04 km^2 in all cases, the rollover value of our inventory; plus/minus values are standard error on the power-law exponent of the regression.

Accepted Article

This article is protected by copyright. All rights reserved.

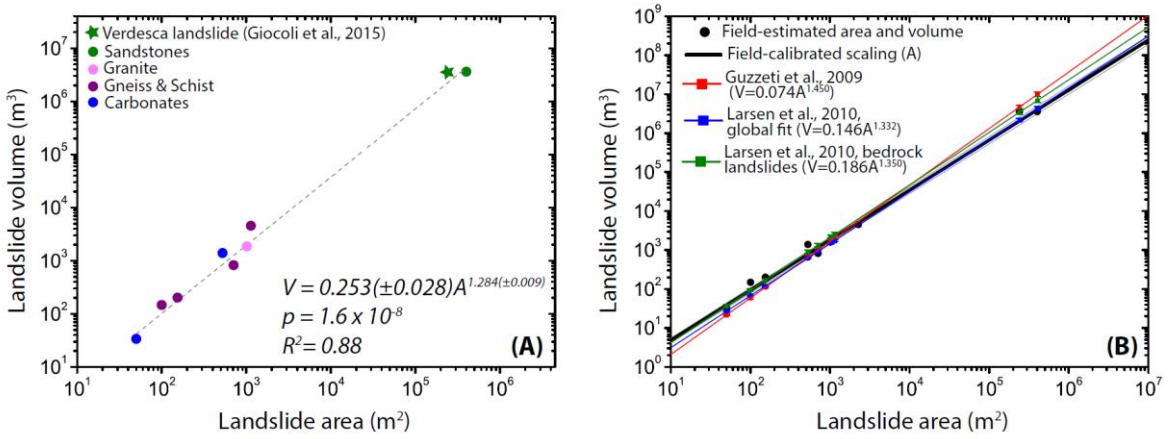


FIGURE 5

Figure 5. (a) Calibration of a landslide area-volume scaling relationship (with standard errors on the parameters estimated for the regression in parenthesis), based on 8 field localities, and on the electric tomography imaging of the Verdesca landslide (Giocoli et al., 2015). (b) Comparison of field-calibrated area-volume scaling from (a) with published area-volume scalings from Larsen et al. (2010) and Guzzetti et al. (2009).

Accepted Article

This article is protected by copyright. All rights reserved.

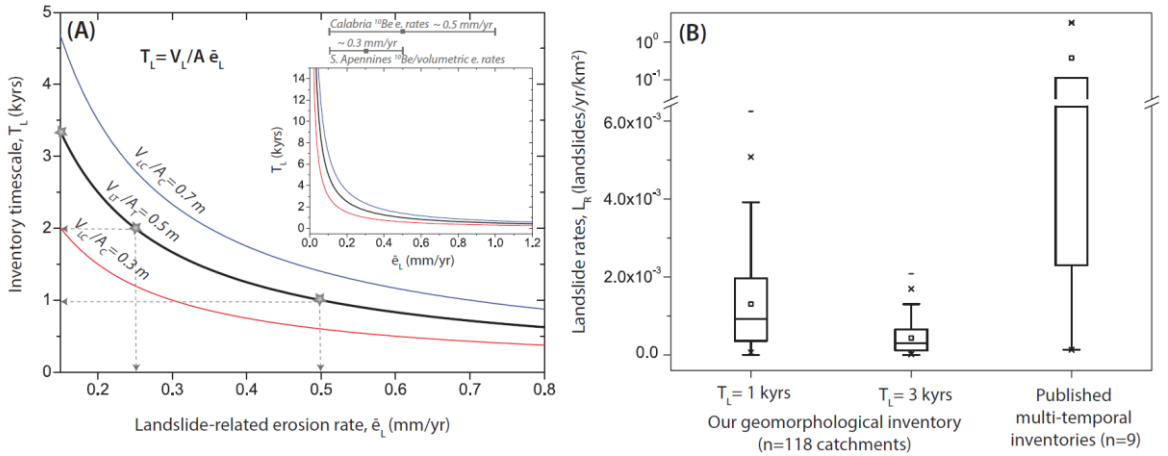


FIGURE 6

Figure 6. (a) Estimated inventory timescale, T_L, for possible values of landslide-related erosion rate, $\bar{e}_L$, for the mean and median V_{LC}/A_C values of the catchments (0.7 m and 0.3 m respectively), and the overall V_{LT}/A_T value for the whole inventory (0.5 m). The inset shows the same curves for a wider range of $\bar{e}_L$ values, together with published cosmogenic nuclide or volumetric erosion rate estimates for the study area (see Geological Setting). (b) Box plots of landslide rates, L_R, calculated for the minimum and maximum plausible T_L values from (a), for all 118 catchments with landslides, and comparison with L_R values that can be inferred from published multi-temporal landslide inventories (see Table S1 in the supplementary material). The line inside the boxes is the median value of the data, and the square is the mean value.

Accepted Article

This article is protected by copyright. All rights reserved.



FIGURE 7

Figure 7. Representative photos of the field localities. (a) Bedrock outcrop, where we measured Schmidt hammer rebound values, and the grain size distributions generated by outcrop weathering (b). (c) Recent landslide, from which we measured the area and volume of the landslide deposit. (d) Landslide deposit grain size. (e) Channel incising footwall catchment, Cittanova Fault (f) Fluvial export grain size.

This article is protected by copyright. All rights reserved.

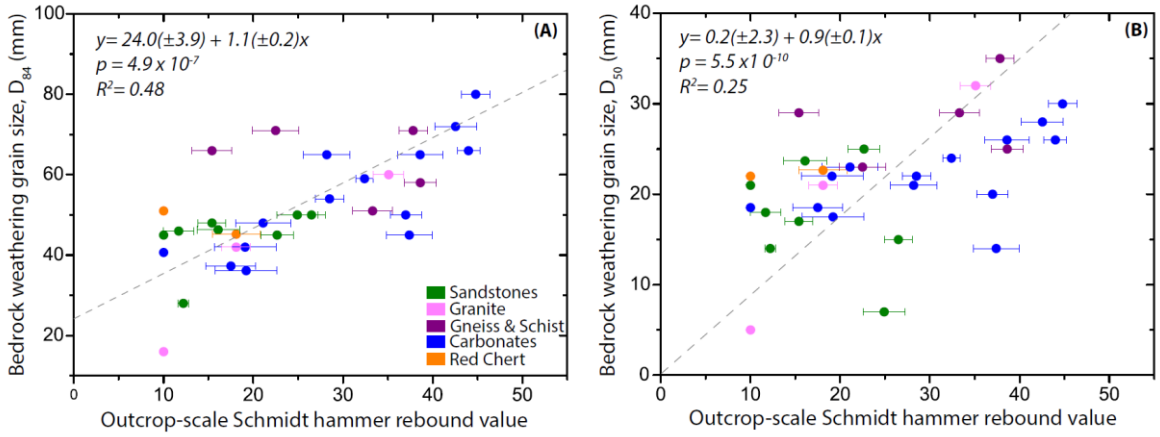


FIGURE 8

Figure 8. D_{84} (a) and D_{50} (b) values of the grain size distributions of bedrock weathering products, plotted against the outcrop-scale mean Schmidt hammer rebound value, from 31 field localities (Table 1). Error bars on the x-axis are the standard error from the mean for the 10 field repeat Schmidt hammer measurements on each outcrop; see methods for error estimates on grain size data. See Fig. 1 for position of field localities, and the supplementary material map for the labelled localities.

Accepted Article

This article is protected by copyright. All rights reserved.

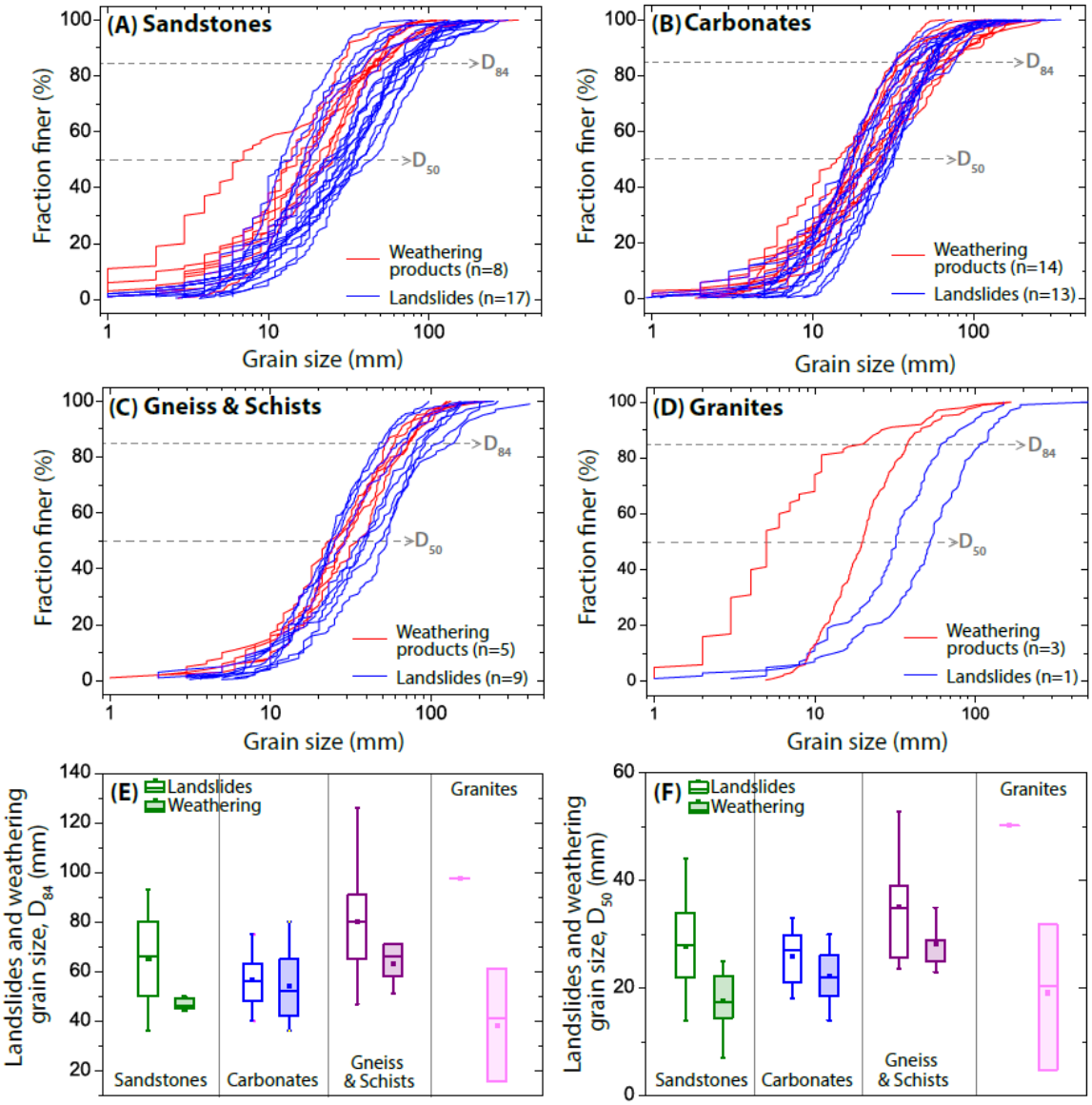


FIGURE 9

Figure 9. Comparison of the cumulative grain size distributions measured from bedrock weathering and landslides, for sandstones (a), carbonates (b), gneisses and schists (c) and granites (d). In (e) and (f), we summarize the D_{50} and D_{84} values of all these distributions in box plots for bedrock weathering and landsliding across all lithologies. See Fig. 1 for position of field localities, and the supplementary material for the labelled localities. The line inside the box plots is the median value of the data, and the square is the mean value.

This article is protected by copyright. All rights reserved.

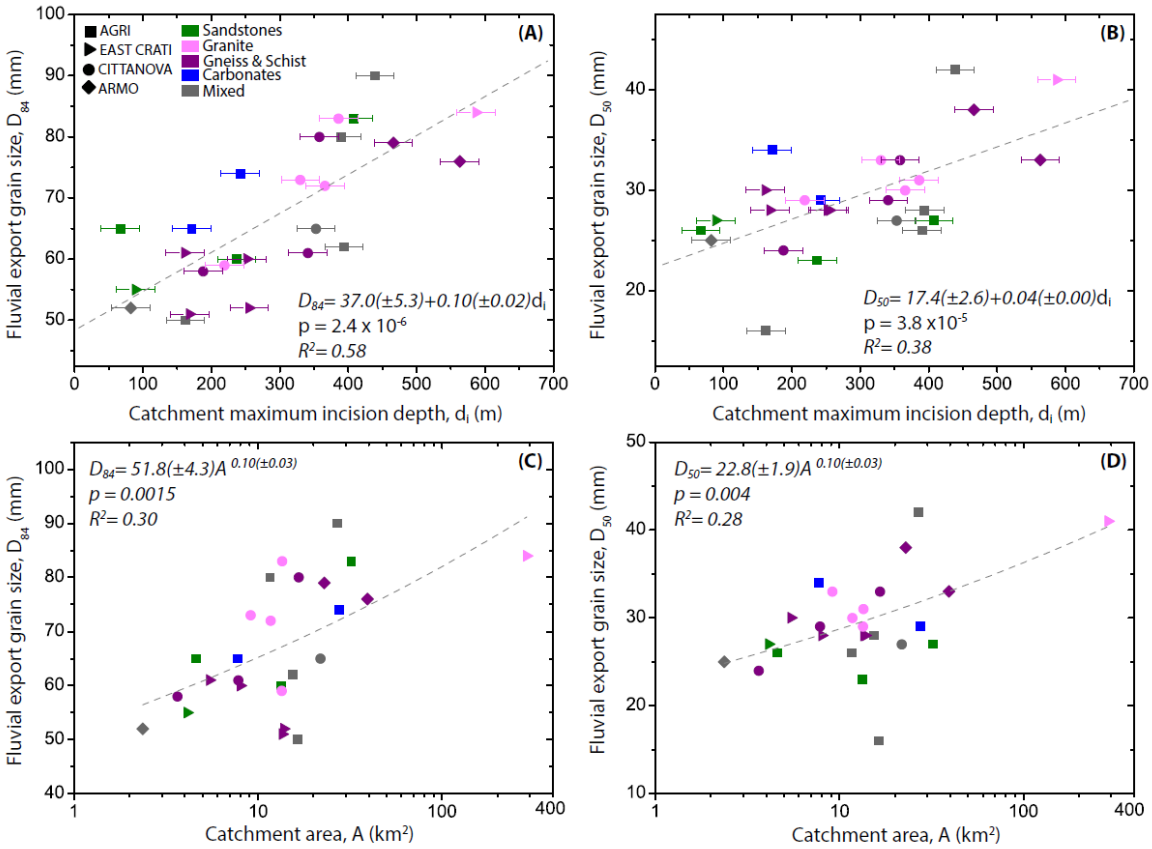


FIGURE 10

Figure 10. D_{84} and D_{50} values for the fluvial export from 26 footwall catchments (see Fig. 1 for localities sites and supplementary material for labelled sites). We compare D_{84} and D_{50} with the catchment maximum incision depth (as a proxy for long-term landslide activity), in (a) and (b), and with the catchments drainage area (as a proxy for discharge), in (c) and (d), respectively. Error bars the incision depth represent ±28 m uncertainty on extracting incision depths; see methods for discussion on errors on D_{84} and D_{50}.

Accepted

This article is protected by copyright. All rights reserved.

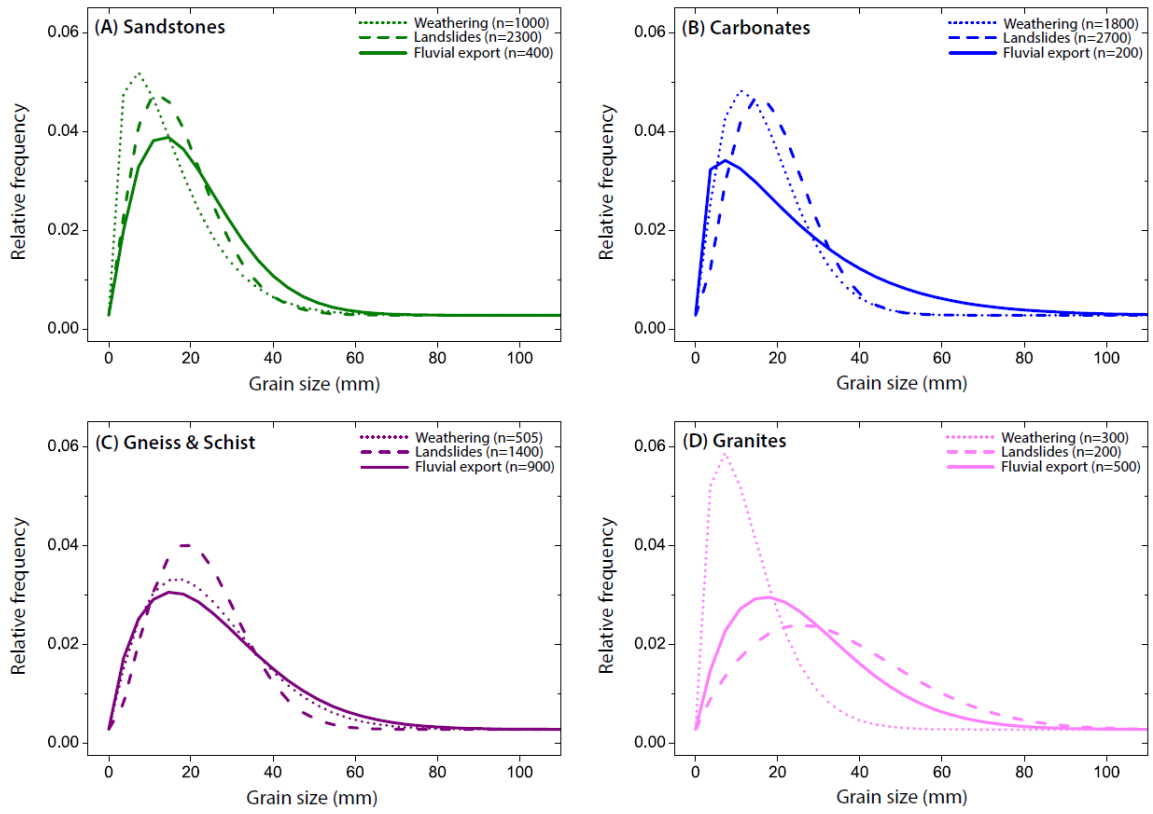


FIGURE 11

Figure 11. Relative frequency of amalgamated grain size fractions supplied by bedrock weathering and landslides, and of the fluvial sediment export; for sandstones (a), carbonates (b), gneisses and schists (c) and granites (d). These represent the combined distributions of all sampling localities for each of these categories and lithologies.

Accepted Article

This article is protected by copyright. All rights reserved.

LITHOLOGICAL CONTROLS ON HILLSLOPE SEDIMENT SUPPLY: INSIGHTS FROM LANDSLIDE ACTIVITY AND GRAIN SIZE DISTRIBUTIONS.

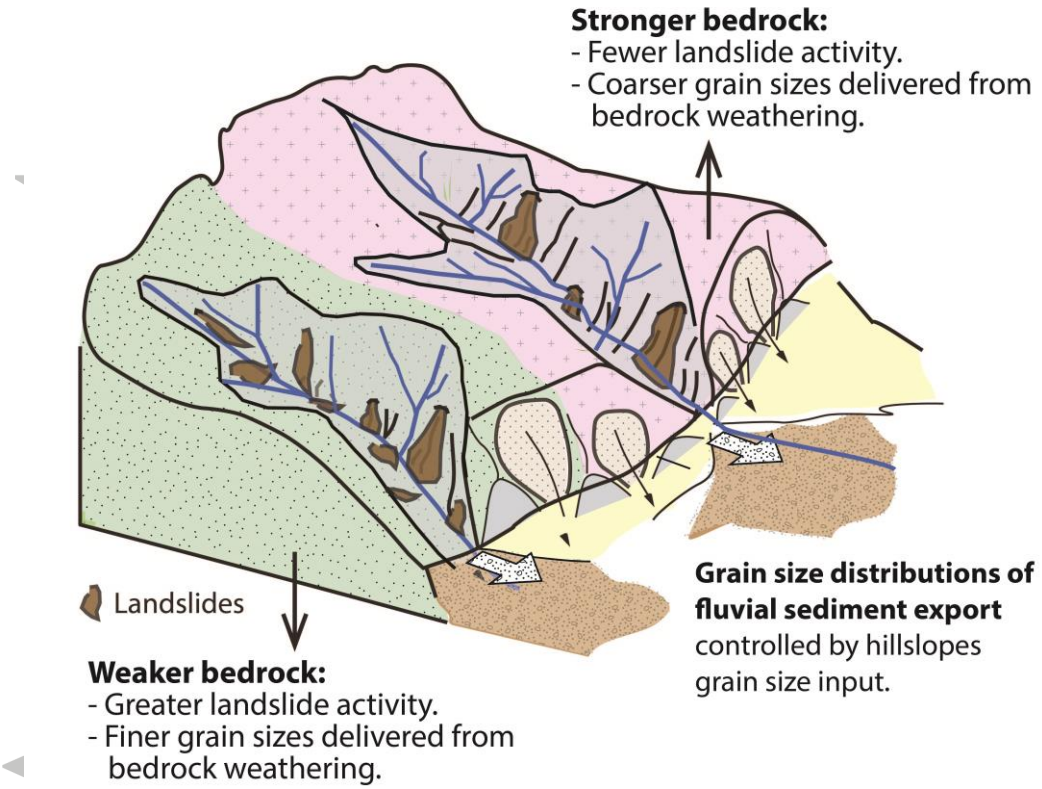
Duna C. Roda-Boluda*, Mitch D'Arcy, Jordan McDonald, Alexander C. Whittaker

* corresponding author: roda@gfz-potsdam.de; dcr12@imperial.ac.uk

Article

- Rock strength and lithology exert a dual control on hillslope sediment fluxes, by modulating several aspects of landslide activity, and the grain size distributions delivered by bedrock weathering and landslides.

- Landsliding in southern Italy is dominated by small-medium, shallow landslides, which generate large landslide densities and play an important role in determining the grain size distributions of catchments' fluvial sediment export.



This article is protected by copyright. All rights reserved.